



## 저작자표시-비영리-변경금지 2.0 대한민국

이용자는 아래의 조건을 따르는 경우에 한하여 자유롭게

- 이 저작물을 복제, 배포, 전송, 전시, 공연 및 방송할 수 있습니다.

다음과 같은 조건을 따라야 합니다:



저작자표시. 귀하는 원저작자를 표시하여야 합니다.



비영리. 귀하는 이 저작물을 영리 목적으로 이용할 수 없습니다.



변경금지. 귀하는 이 저작물을 개작, 변형 또는 가공할 수 없습니다.

- 귀하는, 이 저작물의 재이용이나 배포의 경우, 이 저작물에 적용된 이용허락조건을 명확하게 나타내어야 합니다.
- 저작권자로부터 별도의 허가를 받으면 이러한 조건들은 적용되지 않습니다.

저작권법에 따른 이용자의 권리는 위의 내용에 의하여 영향을 받지 않습니다.

이것은 [이용허락규약\(Legal Code\)](#)을 이해하기 쉽게 요약한 것입니다.

[Disclaimer](#)

Thesis for the Degree of Master of Science

Fluorescence characteristics and dynamics of  
dissolved organic matter (DOM) in the Amundsen  
Sea, Antarctica

by

Juyoung Son

Division of Earth and Environmental System Sciences

The Graduate School

Pukyong National University

February, 2023

Fluorescence characteristics and dynamics of  
dissolved organic matter (DOM) in the Amundsen Sea,  
Antarctica

남극 아문젠해에서 용존 유기 물질의  
형광 특성 및 거동 파악

Advisor: Prof. Mi Ok Park

by

Juyoung Son

A thesis submitted in partial fulfillment of the requirements  
for the degree of

Master of Science

in Division of Earth and Environmental System Science, the Graduate School,  
Pukyong National University

February, 2023

Fluorescence characteristics and dynamics of dissolved organic matter (DOM)  
in the Amundsen Sea, Antarctica

A dissertation

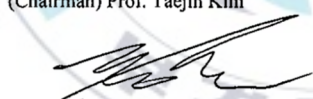
by

Juyoung Son

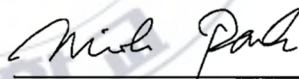
Approved by:



(Chairman) Prof. Taejin Kim



(Member) Ph.D. Jinyoung Jung



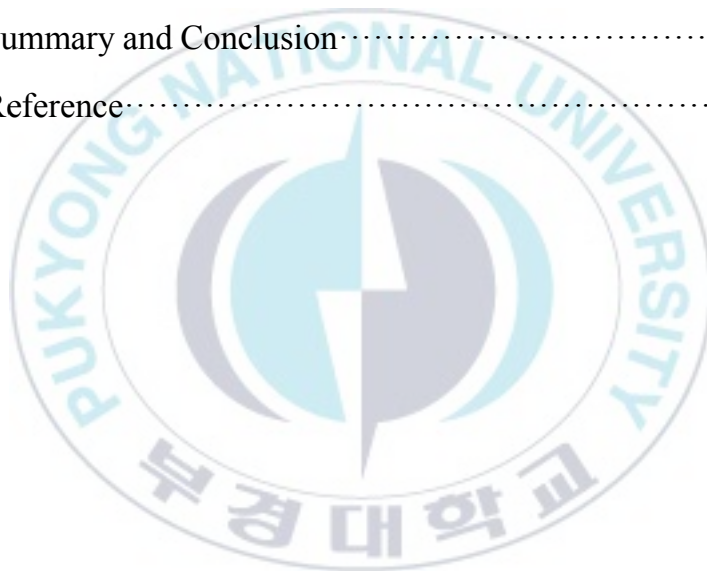
(Member) Prof. Mi Ok Park

February 17, 2023

# Contents

Abstract .....	
List of Tables .....	
List of Figures .....	
Introduction .....	1
Materials and methods .....	5
1. Sampling .....	5
2. Onboard measurements .....	9
3. CDOM analysis .....	10
4. FDOM analysis .....	12
5. POC .....	14
6. DOC .....	15
7. Data analyzes .....	16
Results .....	17
1. Physical and chemical characteristics of the study area .....	17
2. Chl <i>a</i> distribution .....	25
3. POC distribution .....	27
4. DOC distribution .....	29
5. CDOM absorbance distribution .....	31
6. Distribution characteristics of FDOM .....	33
7. Distribution of optical indices of DOM .....	38

. Discussion.....	40
1. Differences in DOM quantity and quality in WGIS and DIS.....	40
2. Sources of humic-like FDOM in the WGIS and DIS.....	46
3. Sources of protein-like FDOM in the WGIS and DIS.....	50
. Summary and Conclusion.....	56
. Reference.....	59



Fluorescence characteristics and dynamics of dissolved organic matter (DOM)  
in the Amundsen Sea, Antarctica

Juyoung Son

Division of Earth and Environmental System Sciences  
The Graduate School, Pukyong National University

**Abstract**

The Amundsen Sea in West Antarctica has undergone a rapid ice loss through basal melting due to the warm Circumpolar Deep Water (CDW) intrusion in the bottom layer. This warm and salty CDW intrusion to the continental shelf drives the basal melting of glaciers. Glacial melt water can supply bioavailable iron to the euphotic zone, which can affect the primary production, resulting in the changes in the dynamics of dissolved organic matter (DOM) and carbon cycle in the Amundsen Sea. Thus, it is important to understand the dynamics and quality of DOM and its sources in the Amundsen Sea. Based on the hydrographic observations conducted in the Amundsen Sea from 6 January to 16 February 2020, the relatively high values of dissolved organic carbon (DOC) and chromophoric

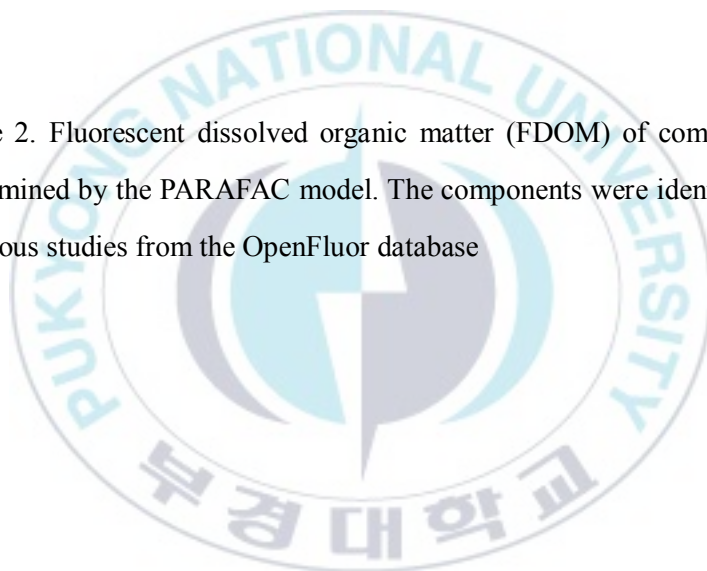
dissolved organic matter (CDOM) absorption coefficient at 350 nm ( $a_{350}$ ) were observed in the WGIS. Additionally, the low value of spectral slope coefficient ( $S_{275-295}$ ) and the high value of specific UV absorbance at 254 nm ( $SUVA_{254}$ ) indicated that the high molecular weight of DOM in the WGIS. On the other hand, the values of  $a_{350}$  and  $SUVA_{254}$  decreased with increasing  $S_{275-295}$  value, indicating that the low molecular weight of DOM was predominant in the DIS. By the fluorescence excitation-emission matrices (EEMs), which analyzed by parallel factor (PARAFAC) modeling, a humic-like component (C1,  $Ex_{max}/Em_{max} = 250/427$ ) and a protein-like component (C2,  $Ex_{max}/Em_{max} = 275/339$ ) were identified. The vertical distribution of C1, a tracer for CDW, suggested that the DIS was more directly influenced by the supply of DOM from sediment origin and glacier meltwater to the euphotic zone due to the intrusion of warm CDW. The supply of DOM by the CDW to the euphotic zone in the DIS can expose DOM to UV radiation, which enhances CDOM photo-degradation in the upper layer. In contrast, the CDW intrusion to the basal glacier in the WGIS was prevented by the Antarctic slope front (ASF), which forms isopycnal gradients in bottom depth. As a result, the distinct regional differences of optical properties between DIS and WGIS occurred. The  $FDOM_H^*$  values, calculated by a significant positive relationship between C1 and apparent oxygen utilization (AOU) ( $r^2=0.45$ ,  $p < 0.05$  in the WGIS, and  $r^2=0.47$ ,  $p < 0.05$  in the DIS), showed positive values, revealing that C1 was derived from sediments in both the WGIS and DIS. In addition, the relationships between C2, nutrient, and particulate organic carbon (POC) suggested that C2 was mainly originated from marine primary production and sea ice or microbial activity origin in both the WGIS and DIS. The results of this study indicate that the differences in the characteristics of DOM between the WGIS and DIS are likely caused by the difference of the CDW intrusion pathway rather than the differences of DOM sources. Therefore, this study suggests that the changes in the CDW intrusion pathway by glacial basal melting and/or global warming may result in the change in DOM quantity and quality in West Antarctica.



## List of Tables

Table 1. The sampling dates, locations of stations depths in the Amundsen Sea during January 2020

Table 2. Fluorescent dissolved organic matter (FDOM) of components determined by the PARAFAC model. The components were identified in previous studies from the OpenFluor database



## List of Figures

Figure 1. Location of the sampling stations in the Amundsen Sea during ANA10B cruise in the West of the Getz Ice Shelf (WGIS) and Dotson Ice Shelf (DIS) in January 2020.

Figure 2. Potential temperature-salinity ( $\theta$ -S) diagram of the sampling stations along the west of the Getz ice shelf (WGIS) (black circle) and the Dotson ice shelf (DIS) (red triangle) in the Amundsen Sea.

Figure 3. Spatial distributions of (a) salinity and (b) temperature ( ) in the WGIS and DIS in the Amundsen Sea. The station numbers are shown at the top of each station.

Figure 4. Vertical profiles of potential temperature ( ) and salinity in WGIS and DIS in this study. In WGIS, data were plotted as grey dots, with a black line that represents the mean value, and the error bar representing standard deviations. In DIS, data were plotted as red dots, with a red line that represents the mean value, and the error bar representing standard deviations.

Figure 5. Vertical distributions of (a) nitrate and nitrite ( $\mu\text{mol/L}$ ) ( $\text{NO}_3+\text{NO}_2$ ), (b) phosphate ( $\text{PO}_4$ ), (c) silicic acid ( $\text{Si(OH)}_4$ ), and (d) ammonium ( $\text{NH}_4$ ) in the WGIS and DIS in this study.

Figure 6. The vertical patterns of AOU ( $\mu\text{mol/kg}$ ) in the WGIS and DIS in this study.

Figure 7. The (a) spatial and (b) vertical profiles of Chl *a* ( $\text{mg/m}^3$ ) in the WGIS and DIS. The station numbers are shown at the top of each station. The white dotted lines and white solid lines indicate the euphotic zone depth (EZD) and the mixed layer depth (MLD), respectively.

Figure 8. The (a) spatial and (b) vertical profiles of POC ( $\mu\text{M C}$ ) in the WGIS and DIS in the Amundsen Sea.

Figure 9. The (a) spatial and (b) vertical profiles of DOC ( $\mu\text{M C}$ ) in the WGIS and DIS in the Amundsen Sea.

Figure 10. The (a) spatial and (b) vertical profiles of  $a_{350}$  ( $\text{m}^{-1}$ ) in the WGIS and DIS in the Amundsen Sea.

Figure 11. EEM contour plots of the fluorescent spectra of the two components (a) C1 ( $E_{x_{max}}/E_{m_{max}}$ : 250/427, R.U.) and (b) C2 ( $E_{x_{max}}/E_{m_{max}}$ : 275/339, R.U.), identified by PARAFAC analysis in the seawater samples with excitation-emission matrix spectroscopy (EEMs) for all the samples. (c) Loading of C1 and (d) loading of C2 were shown with the blue solid lines representing the excitation wavelength and the orange solid lines representing the emission wavelength.

Figure 12. Spatial distributions of (a) C1, and (b) C2 along the west of the Getz ice shelf (WGIS) and the Dotson ice shelf (DIS) in the Amundsen Sea.

Figure 13. Vertical profiles of  $S_{275-295}$  ( $\text{nm}^{-1}$ ),  $\text{SUVA}_{254}$  ( $\text{L mg C}^{-1} \text{m}^{-1}$ ), and HIX in the WGIS and DIS in the Amundsen Sea.

Figure 14. The scatter plot of CDOM absorption coefficient at 350 nm ( $a_{350}$ ,  $\text{m}^{-1}$ ) and CDOM exponential slope values between 275-295 nm ( $S_{275-295}$ ,  $\text{nm}^{-1}$ ). Black dots represent the data of WGIS, and red triangles represent the data of DIS.

Figure 15. The summary of the oceanic, atmospheric and geologic controls influencing glaciological change along (a) Getz Ice Shelf and (b) the region west of 135 °W (Christie et al., 2018).

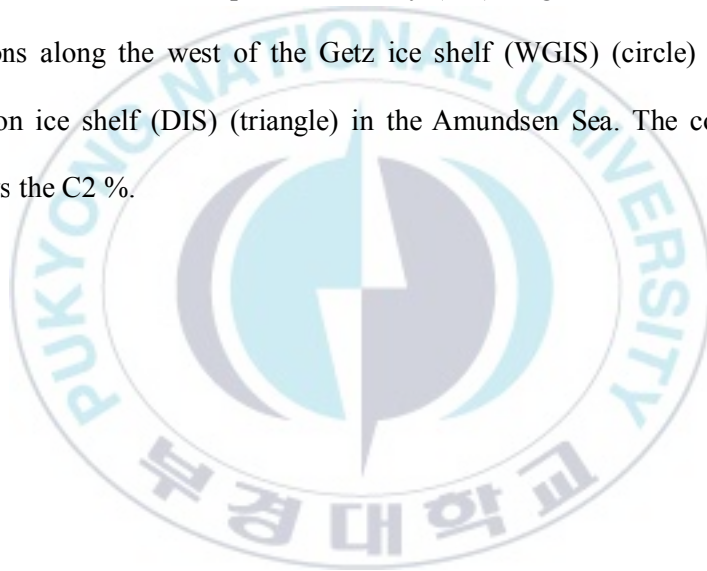
Figure 16. Correlations between C1 (R.U.) and AOU ( $\mu\text{mol/kg}$ ) in the mesopelagic layer (200m–1000m) in WGIS ( $C1 = 0.9 \times 10^{-4} \text{AOU} + 9.54 \times 10^{-3}$ ,  $r^2 = 0.45$ ) and DIS ( $C1 = 0.6 \times 10^{-4} \text{AOU} + 1.3 \times 10^{-2}$ ,  $r^2 = 0.47$ ). Black circles represent the samples in WGIS, and red triangles represent the samples in DIS. The reference equation 3 was represented with a green line.

Figure 17. Spatial distributions of  $\text{FDOM}_H^*$  along the WGIS and DIS in the Amundsen Sea in Antarctica. Data of autochthonous  $\text{FDOM}_H$  and  $\text{FDOM}_H^*$  in the upper 200 m is omitted from the figures since it is affected by the air-sea gas exchange of oxygen.

Figure 18. Correlations between C2 % and  $\text{PO}_4$  ( $\mu\text{mol/L}$ ) in the WGIS (circle) and DIS (triangle) in the Amundsen Sea in Antarctica. The color bar shows the POC ( $\mu\text{M C}$ ) concentration.

Figure 19. Correlations between POC ( $\mu\text{M C}$ ) and Chl a ( $\text{mg}/\text{m}^3$ ) ( $y = 3.6228x + 9.9747$ ,  $r^2 = 0.8793$ ) in the WGIS and DIS in the Amundsen Sea in Antarctica.

Figure 20. Potential temperature-salinity ( $\theta$ -S) diagram of the sampling stations along the west of the Getz ice shelf (WGIS) (circle) and the Dotson ice shelf (DIS) (triangle) in the Amundsen Sea. The color bar shows the C2 %.



## **. Introduction**

The Southern Ocean (south of 50 °S) is considered to be the strongest sink of anthropogenic carbon (Sabine et al., 2004; Takahashi et al., 2009; Frölicher et al., 2015). Recently the extent of sea ice has decreased because of the rapid climate changes in the Southern Ocean (Thomas et al., 2004; Cavalieri and Parkinson, 2008; Rignot et al., 2008; Turner et al., 2009; Pritchard et al., 2012). Especially, the Western Antarctic is considered as the region of sensitivity to climate change (Jacobs and Comiso, 1997; Stammerjohn et al., 2012; Criscitiello et al., 2013). The Amundsen Sea located in the western Antarctica and is known as the most productive polynyas around Antarctica (Arrigo et al., 2012). This region is experiencing a rapid rate of decrease in sea ice concentration, ice retreat, and glacial melting that resulted in the sea level rises (Rignot et al., 2008; Pritchard et al., 2012; Stammerjohn et al., 2012). The main driver of these recent sea ice and glaciers melting has been addressed to be the intrusion of warm and salty circumpolar deep water (CDW) that circulates around the Antarctic (Jacobs et al., 1996; Walker et al., 2007; Jenkins et al., 2010; Pritchard et al., 2012; Ha et al., 2013; Kim et al., 2017). This relatively warm and salty CDW intrusion to the continental shelf drives the basal

melting of floating glaciers and thinning of the outlet glaciers (Walker et al., 2007; Jenkins et al., 2010). This melting by rapid climate change can be attributed to the meltwater spreading, biogeochemical cycle, and freshening of Antarctic coastal water that influences the Antarctic Bottom Water (AABW) formation (Thurnherr et al., 2014). The Amundsen Sea Polynya (ASP) was reported as the most productive polynyas among the coastal polynyas around Antarctica (Arrigo and van Dijken, 2003; Arrigo et al., 2012). Glacial melt water supplies not only bioavailable iron but also dissolved organic matter (DOM) (Stedmon et al., 2011; Yager et al., 2012; Brogi et al., 2018) to the ASP and affects the primary production and carbon cycle in the Amundsen Sea. So, knowledge of the distribution and characteristics of DOM is important.

In the recent DOM studies in the Amundsen Sea in Southern Ocean are reported relationship between heterotrophic microbial processes and dissolved organic carbon (DOC) cycle in glacier meltwater (Min et al., 2022), and Kim et al. (2022) reported how heterotrophic metabolic response affects the biological carbon pump. The ecological importance of viral Lysis by phytoplankton which effect to the microbial food web, and carbon export was reported by Eich et al. (2022). Lee et al. (2016) reported the relationship between the phytoplankton composition and the CDOM production, and Chen et al. (2019) reported the production of



tyrosine-like fluorescence and labile CDOM by primary productivity. Also, Jeon et al. (2021) traced the CDW circulation and glacial meltwater distribution by using humic-like FDOM to understand the DOC dynamic. Despite these studies, the characteristics and the dynamics of the DOM are still poorly understood. In particular, there is little known about DOM in front of the West Getz Ice Shelf.

The chromophoric dissolved organic matter (CDOM), the coloured fraction of DOM, can be an optically important constituent in ocean environment because it absorbs ultra-violet and visible light. Light absorption by CDOM can implicate the primary production by reducing the light availability for phytoplankton, and influencing the euphotic zone (Osburn et al., 2009). Because CDOM can absorb solar radiation, they may also contribute to the thermodynamics of the upper ocean (Kirk, 1988; Granskog et al., 2007). CDOM can play important roles in biogeochemical and physical processes in the ocean. So, it is important to understand the distribution of DOM and its sources in the Amundsen Sea which is one of the most rapidly warming regions on Earth (Bromwich et al., 2013).

Absorption spectra analysis of CDOM can use to understand the DOM cycling in aquatic ecosystems (Bricaud et al., 1981). The absorption coefficient ( $a_{CDOM}$ ) and CDOM spectral slope (S) can recognize proxies of CDOM concentration and molecular weight (Helms et al., 2008).

Fluorescent dissolved organic matter (FDOM) is a fraction of the CDOM, which has different optical properties depending on the molecular structure of the DOM. These properties can allow us to identify the fluorescence characteristics and sources of DOM. Also, to characterize the properties of DOM, specific UV absorbance ( $SUVA_{254}$ ) can use indices such as which indicates DOM aromaticity (Weishaar et al., 2003).

These research areas are located in the West of Getz Ice Shelf (WGIS), and in the Dotson Ice Shelf (DIS) which are influenced by the circulation of DOM due to ice shelf loss due to rapid climate change. Here, three-dimensional fluorescence excitation-emission matrices (EEMs) were analyzed by parallel factor (PARAFAC) modeling to understand the regional characteristics of DOM in the Amundsen Sea. The objective of this study is to investigate the fluorescence characteristics and dynamics of DOM in front of the West of Getz Ice Shelf (WGIS) and Dotson Ice Shelf (DIS) in the Amundsen Sea. So, hydrographic characteristics of the water column, concentrations of DOC, and optical properties of DOM were identified. In addition, the source of DOM was identified by using the optical properties of DOM.

## **. Materials and methods**

### **2.1 Sampling**

The sampling stations is shown in Figure 1. Stations are located in the West of the Getz ice shelf (WGIS) and Dotson Ice Shelf (DIS) in the Amundsen Sea in West Antarctica. Sea water samples and environmental data were collected aboard in the Korean icebreaker research vessel (IBR/V), Araon from January 6 to February 16 in 2020 (ANA10B) (Figure 1). Sampling was conducted at 22 stations during the cruise in the WGIS and DIS. The sampling dates, locations of sampling sites, and station depths are listed in Table 1.

At all the stations, seawater samples were collected using a rosette sampler equipped with 24 – 10 L Niskin bottles, and hydrographic information (temperature, salinity) was obtained from the conductivity-temperature-depth (CTD) sensors (Sea-Bird Electronics, SBE 911 plus). The mixed layer depth (MLD) was estimated from CTD density profiles and is defined as the depth at which the density change exceeded  $0.05 \text{ kg m}^{-3}$  relative to the reference value at a 10 m depth (Venables and Moore, 2010). The euphotic zone depth (EZD) is defined as the depth at which photosynthetically available radiation (PAR) was 1 % (Kirk, 1994).

Apparent oxygen utilization (AOU) was calculated as a difference between measured DO concentrations and its equilibrium saturation. AOU was calculated below 50 m because the exchange of oxygen between the ocean and the atmosphere strongly influences the accurate estimation of AOU.



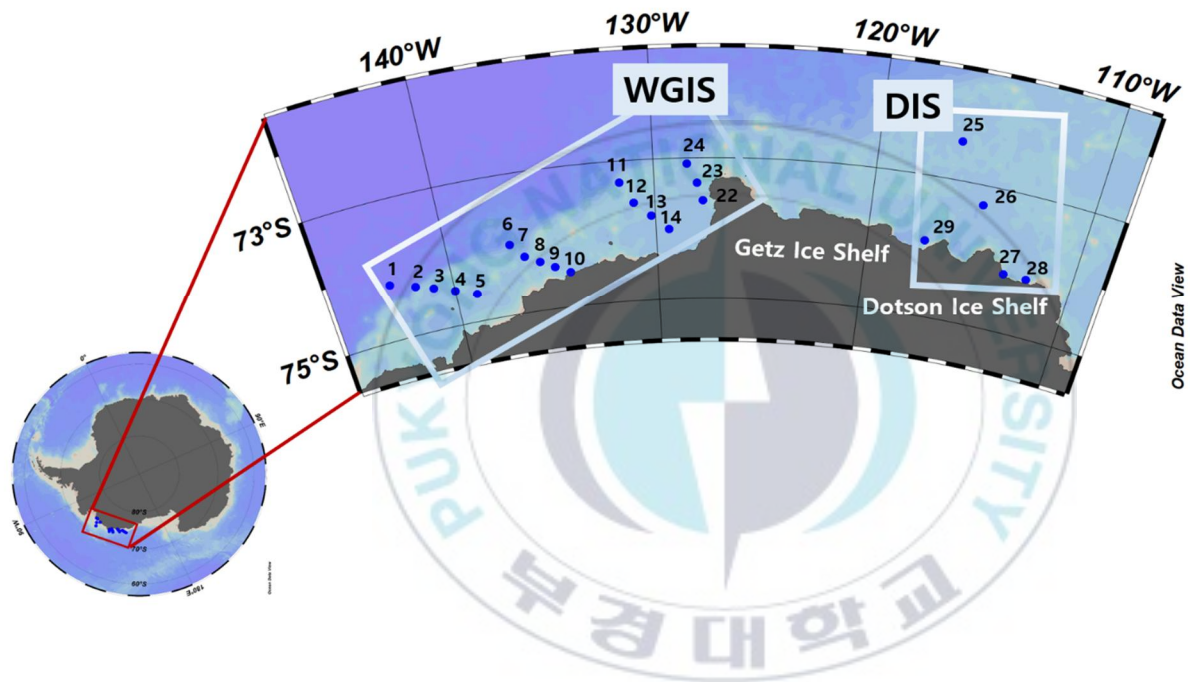


Figure 1. Location of the sampling stations in the West of the Getz Ice Shelf (WGIS) and Dotson Ice Shelf (DIS) in the Amundsen Sea during ANA10B cruise.

Table. 1

The sampling dates, locations of stations depths in the Amundsen Sea during January 2020

station	Date	Latitude	Longitude	depth (m)	MLD (m)	EZD (m)
1	01/06/2020	-74.20	-143.00	3607	40	31
2	01/06/2020	-74.32	-141.83	2206	30	19
3	01/06/2020	-74.40	-141.00	431	30	18
4	01/06/2020	-74.50	-140.00	550	23	28
5	01/06/2020	-74.60	-139.00	705	42	54
6	01/08/2020	-74.00	-137.00	2319	24	13
7	01/08/2020	-74.20	-136.40	557	16	13
8	01/09/2020	-74.30	-135.70	488	16	12
9	01/09/2020	-74.40	-135.00	617	23	11
10	01/09/2020	-74.50	-134.30	465	30	13
11	01/09/2020	-73.30	-131.60	429	14	26
12	01/09/2020	-73.60	-131.00	500	19	15
13	01/09/2020	-73.80	-130.20	582	15	12
14	01/10/2020	-74.00	-129.40	707	20	11
22	01/23/2020	-73.60	-127.80	527	30	12
23	01/23/2021	-73.35	-128.05	616	25	11
24	01/23/2022	-73.08	-128.49	558	23	13
25	01/27/2020	-72.44	-116.46	553	13	na
26	01/27/2020	-73.28	-114.96	832	37	24
27	01/28/2020	-74.17	-113.33	532	32	11
28	01/28/2020	-74.17	-112.20	790	47	12
29	02/16/2020	-73.92	-117.29	777	80	na

\* na: not available

## 2.2 Onboard measurements

Seawater samples for inorganic nutrients, including nitrate and nitrite ( $\text{NO}_3+\text{NO}_2$ ), phosphate ( $\text{PO}_4$ ), silicic acid ( $\text{Si}(\text{OH})_4$ ), and ammonium ( $\text{NH}_4$ ), were drawn from the Niskin rosette into a 50 mL conical tube, and immediately stored in a 4 °C refrigerator prior to chemical analysis. Inorganic nutrients were determined by using a four-channel continuous Auto-Analyzer (QuAatro, Seal Analytical) according to the Joint Global Ocean Flux Study (JGOFS) protocols described by Gordon et al. (1993). The precision of the analysis procedures for the  $\text{NO}_3+\text{NO}_2$ ,  $\text{PO}_4$ ,  $\text{Si}(\text{OH})_4$ , and  $\text{NH}_4$  were  $\pm 0.14$ ,  $\pm 0.02$ ,  $\pm 0.28$ , and  $\pm 0.18 \mu\text{mol kg}^{-1}$ , respectively.

Seawater samples for chlorophyll *a* (Chl *a*) were collected in the upper 200 m and prefiltered through a precombusted (at 550 °C for 6h) Whatman GF/F filter. Chl *a* was extracted 90 % acetone for 24 h and measured onboard using a fluorometer (Trilogy, Turner Designs, USA).

### 2.3 CDOM analysis

Seawater samples for CDOM absorbance analysis were drawn from the Niskin bottle by gravity filtration through an inline precombusted (at 550 °C for 6 h) Whatman GF/F filter (47 mm, 0.45  $\mu\text{m}$  pore) which was held in an acid-cleaned (0.1 M HCl) polycarbonate 47 mm filter holders (PP-47, ADVANTEC). This filter holder was attached directly to the Niskin bottle spigot. The filtering systems were rinsed with the seawater sample before its collection and collected in a 200 mL acid-cleaned glass bottle. Samples were immediately distributed into two pre-combusted 20 mL glass ampoules (at 550 °C for 6 h) with a sterilized serological pipette. The glass ampoules were sealed with a torch, quickly frozen, and preserved at  $-24$  °C freezer until analysis.

Spectra of CDOM absorbance was measured throughout the UV–visible spectrophotometer (Shimadzu UV–2600, Japan) with a 1 cm quartz cuvette using Milli-Q water as a reference. Spectra were performed between 200 and 800 nm every 1.0 nm intervals with a slow scan speed in duplicate and then averaged. CDOM absorbance spectra were corrected for the residual absorbance at 750 nm by subtracting where organic matter absorption rarely occurs. The corrected CDOM absorption coefficient ( $a_{\lambda}$ ) was converted into absorption coefficients using the following equation:



$$a(\lambda) = 2.303 \times \frac{A(\lambda)}{l} \quad (1)$$

where the  $a(\lambda)$  is the Napierian absorbance coefficient ( $\text{m}^{-1}$ ) at a specific wavelength ( $\lambda$ , in nm), 2.303 is the conversion factor from  $\log_{10}$  to  $\log$  units, and  $l$  is the length of the optical path in meters (here 0.01 m) (Blough and Green, 1995; Kahru and Mitchell, 2001). The absorption coefficient ( $a_\lambda$ ) was calculated at 350 nm ( $a_{350}$ ). In this study,  $a_{350}$  was chosen to describe the quantity of CDOM.

The slope coefficient of the CDOM absorption spectrum,  $S$  ( $\text{nm}^{-1}$ ), was calculated using the following equation:

$$a(\lambda) = a(\lambda_0) \times e^{-S(\lambda-\lambda_0)} \quad (2)$$

where the  $a(\lambda_0)$  is the absorption coefficient at a reference wavelength ( $\text{m}^{-1}$ ),  $S$  is the slope ( $\text{nm}^{-1}$ ), and the spectral slope coefficient in the  $\lambda - \lambda_0$  nm spectral range (Bricaud et al., 1981). The  $S$  value was estimated at the 275–295 nm spectral range ( $S_{275-295}$ ).  $S_{275-295}$  is characterized by the highest variations and this spectrum offers an indication of a reliable proxy of CDOM molecular weight, photobleaching, and DOM source in the marine environment (Carder et al., 1989; Helms et al., 2008; Fichot and Benner, 2012).

## 2.4 FDOM analysis

Seawater samples for FDOM analysis were collected in the same way as CDOM sampling. Filtered samples were collected in glass ampoules, sealed with a torch, and stored at dark – 20 °C freezer until the analysis.

Three-dimensional fluorescence excitation-emission matrices (EEMs) were conducted using a Hitachi F-7100 luminescence spectrometer. EEMs analysis was conducted by detecting emission wavelengths (Em) of 280–550 nm at 1 nm intervals, and excitation wavelengths (Ex) of 250–500 nm at 5 nm intervals. The scan speed was 12000 nm/min. The Milli-Q water was used as a blank. The EEMs were corrected for the inner filter effect by diluting with Milli-Q water when the sample was higher than 0.3 cm<sup>-1</sup> at 254 nm (Lakowicz, 1999; Zepp et al., 2004). The Raman Unit (R.U.) normalization was conducted by subtracting the Milli-Q water measured in the same conditions from the EEMs and integrating the Raman-integrated area from 380 to 420 nm at 350 nm excitation (Stedmon et al., 2003). The EEMs were elaborated with the parallel factor (PARAFAC) modeling by using MATLAB with the DOM Fluor toolbox (Stedmon and Bro, 2008). The number of components was determined based on split-half validation.

The relative abundances of each fluorescent component were

determined by dividing each component fluorescent intensity by total fluorescence intensity (e.g.,  $C2 \% = C2 / (C1 + C2) \times 100$ ). The source of humic-like FDOM (FDOM<sub>H</sub>) in marine environments can be separated into autochthonous DOM and allochthonous DOM. A general linear relationship between FDOM<sub>H</sub> and AOU was the result of the in situ production of FDOM<sub>H</sub> during oxygen consumption by microbial degradation (Hayase and Shinozuka, 1995; Yamashita et al., 2007; Yamashita and Tanoue, 2008; Jørgensen et al., 2011; Catalá et al., 2015; Yamashita et al., 2020). The FDOM<sub>H</sub>-AOU relationship observed in the bathypelagic layer is very similar to that observed in the global ocean (Jørgensen et al., 2011). So, autochthonous FDOM<sub>H</sub> was determined by the linear regression between AOU and FDOM<sub>H</sub> which is produced by consuming the oxygen, and allochthonous FDOM<sub>H</sub> (FDOM<sub>H</sub><sup>\*</sup>) was estimated by the following equation by Yamashita (2020):

$$\text{autochthonous FDOM}_H = 1.54 \times 10^{-5} \times \text{AOU} + 2.17 \times 10^{-3} \quad (3)$$

$$\text{FDOM}_H^* = \text{FDOM}_H - \text{autochthonous FDOM}_H \quad (4)$$

Samples in the upper 200 m was excluded when calculating autochthonous FDOM<sub>H</sub> and FDOM<sub>H</sub><sup>\*</sup> values because the abundance of FDOM<sub>H</sub> is controlled by photodegradation from sunlight in the surface layer, and AOU is controlled by air-sea gas exchange.

## 2.5 POC

For particulate organic carbon (POC) analyses, seawater samples were drawn from the Niskin bottle into an amber polyethylene bottle. 1–2 L of seawater samples were filtered on a pre-combusted (at 550 °C for 6 h) GF/F filter (47 mm, 0.45 µm pore; Whatman) with a gentle vacuum at 0.1 < MPa. Before analysis in the land laboratory, the filters were stored at – 80 °C deep freezer.

The filters were freeze-dried overnight at – 80 °C deep freezer and acidified by HCl fuming in a desiccator until 24 h to remove inorganic carbon as described by Jung et al. (2020). The acidified samples were neutralized by NaOH with silica gel in a desiccator and kept in a vacuum for 24 h. Samples were measured by CHN elemental analyzer (Vario MACRO cube, Elementar, Germany). Acetanilide was used as a standard. The analytical precision was  $\pm 4 \%$ .

## 2.6 DOC

Seawater samples for dissolved organic carbon (DOC) were collected in the same way as CDOM sampling. DOC concentrations were measured by high-temperature combustion using a Shimadzu TOC-L analyzer. DOC concentrations were corrected with the 18.2 M $\Omega$  ultrapure Milli-Q (Millipore) water and consensus reference material (CRM, 42–45  $\mu$ M C, deep Florida Strait water obtained from the University of Miami). CRM was measured every sixth analysis to check the accuracy of the measurements and analytical errors of samples were in agreement within 5%.

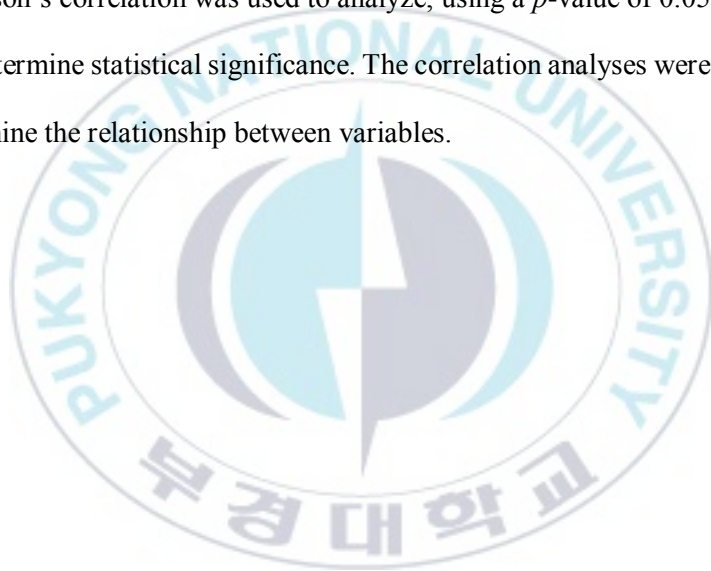
The carbon-specific UV absorbance (SUVA) is defined as the UV absorbance of a water sample at a given wavelength normalized for DOC concentration (Weishaar et al., 2003). Specific UV absorbance at 254 nm (SUVA<sub>254</sub>) was calculated as:

$$\text{SUVA}_{254} = \frac{a_{254}}{\text{DOC}} \quad (5)$$

SUVA<sub>254</sub> (L mg C<sup>-1</sup> m<sup>-1</sup>) has been reported that it was commonly used as an indicator of aromaticity of aquatic humic substances (Westerhoff et al., 2004). As SUVA<sub>254</sub> is 3 or higher than the DOC is composed largely of the high aromaticity of DOC (Berggren et al., 2009; Asmala et al., 2013).

## 2.7 Data analyzes

Statistical analyzes were performed with SPSS 12.0 (Statistical Program for Social Sciences) software was used for statistical analysis. Pearson's correlation was used to analyze, using a  $p$ -value of 0.05 or 0.01 to determine statistical significance. The correlation analyses were used to examine the relationship between variables.



## **. Results**

### **3.1 Physical and chemical environmental characteristics of the study area**

The sampling dates, location and depth of sampling stations are presented in Table 1. Four different water masses were identified by the potential temperature-salinity ( $\theta$ -S) diagrams (Figure 2): Antarctic Surface Water (AASW), Winter Water (WW), modified CDW (mCDW), and Circumpolar Deep Water (CDW) (Jacobs et al., 2012; Yager et al., 2012). CDW, with high temperature ( $>1^\circ\text{C}$ ) and high salinity ( $>34.7$ ), is sourced from the Antarctic Circumpolar Current (ACC) that flows close to the continental margin (Orsi et al., 1995). In this study, CDW was observed at depths of  $>500$  m. mCDW ( $0-1^\circ\text{C}$ ,  $S < 34.6$ ) originates from the CDW which intrudes into the shelf through glacier-carved troughs. mCDW was observed above the depth of the CDW. WW ( $< -1.7^\circ\text{C}$ ,  $S < 34.1$ ) is the coldest and saline water mass that overlies the mCDW (about 200–400 m in this study), formed through sea ice production during the previous winter. When the sea ice starts to melt, the upwelling of freshened and warmed water of WW becomes AASW. The AASW ( $-1.7 < T < 0^\circ\text{C}$ ,  $S < 34.1$ ) was observed in the upper 200 m.

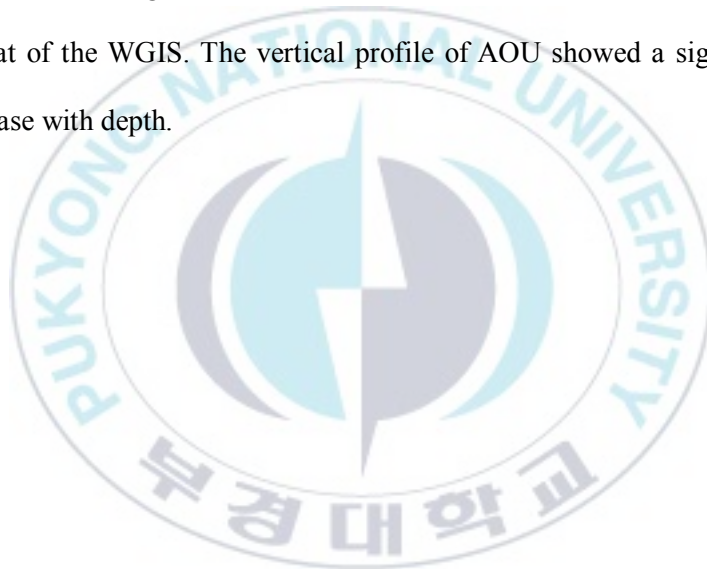
On all profiles, the range of salinity (Figure 3a) and potential temperature (Figure 3b) were from 33.29 to 34.72 and from  $-1.82$  to  $1.73$ , respectively. And the vertical distribution of potential temperature and salinity was shown in Figure 4. The mixed layer depth (MLD) ranged from 13 m to 80 m with a mean of  $28.59 \pm 14.85$  m (Table 1). The deepest MLD was shown at station 29, and the shallowest MLD was shown at station 25. The range of the euphotic zone depth (EZD) was from 11 m to 54 m with a mean of  $17.95 \pm 10.55$  m (Table 1).

The profiles of inorganic nutrients ( $\text{NO}_3+\text{NO}_2$ ,  $\text{PO}_4$ ,  $\text{Si(OH)}_4$ , and  $\text{NH}_4$ ) are presented in Figure 5. In WGIS, the concentrations of  $\text{NO}_3+\text{NO}_2$ ,  $\text{PO}_4$  and  $\text{Si(OH)}_4$  ranged from 2.08 to 34.27  $\mu\text{M}$  (mean:  $28.12 \pm 6.93$   $\mu\text{M}$ ), 0.64–2.34  $\mu\text{M}$  (mean:  $2.01 \pm 0.35$   $\mu\text{M}$ ), and 78.02–138.11  $\mu\text{M}$  (mean:  $89.60 \pm 8.77$   $\mu\text{M}$ ), respectively (Figure 5). Compared to other inorganic nutrients, ammonium concentration was relatively low from 0.01 to 1.36  $\mu\text{M}$  (mean:  $0.39 \pm 0.27$   $\mu\text{M}$ ) (Figure 5d). In DIS, the concentrations of  $\text{NO}_3+\text{NO}_2$ ,  $\text{PO}_4$ ,  $\text{Si(OH)}_4$ , and  $\text{NH}_4$  ranged from 1.04 to 33.67  $\mu\text{M}$  (mean:  $25.66 \pm 10.32$   $\mu\text{M}$ ), 0.43–3.42  $\mu\text{M}$  (mean:  $1.91 \pm 0.66$   $\mu\text{M}$ ), 64.01–104.12  $\mu\text{M}$  (mean:  $91.00 \pm 9.68$   $\mu\text{M}$ ), and 0.01–5.15  $\mu\text{M}$  (mean:  $1.26 \pm 1.43$   $\mu\text{M}$ ), respectively (Figure 5). Vertical profiles of major inorganic nutrients ( $\text{NO}_3+\text{NO}_2$ ,  $\text{PO}_4$ , and  $\text{Si(OH)}_4$ ) showed the lowest values in the surface layer, and increased as the depth increase (Figure 5). However, the profile



of  $\text{NH}_4$  showed no distinct patterns in the water column.

AOU concentrations ranged from 3.54 to 150.92  $\mu\text{mol/kg}$  with a mean value of  $88.27 \pm 30.21$   $\mu\text{mol/kg}$  in WGIS. In DIS, AOU concentrations ranged from 23.69–141.94 with a mean value of  $104.21 \pm 30.79$   $\mu\text{mol/kg}$ . In the DIS, the higher AOU values were shown in 100–400 m compared to that of the WGIS. The vertical profile of AOU showed a significant increase with depth.



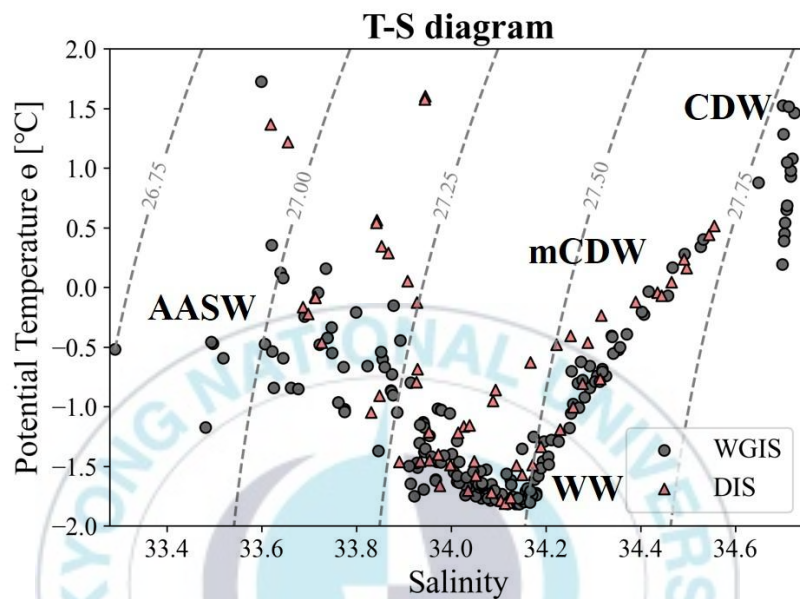


Figure 2. Potential temperature-salinity ( $\theta$ -S) diagram of the sampling stations along the west of the Getz ice shelf (WGIS) (black circle) and the Dotson ice shelf (DIS) (red triangle) in the Amundsen Sea.

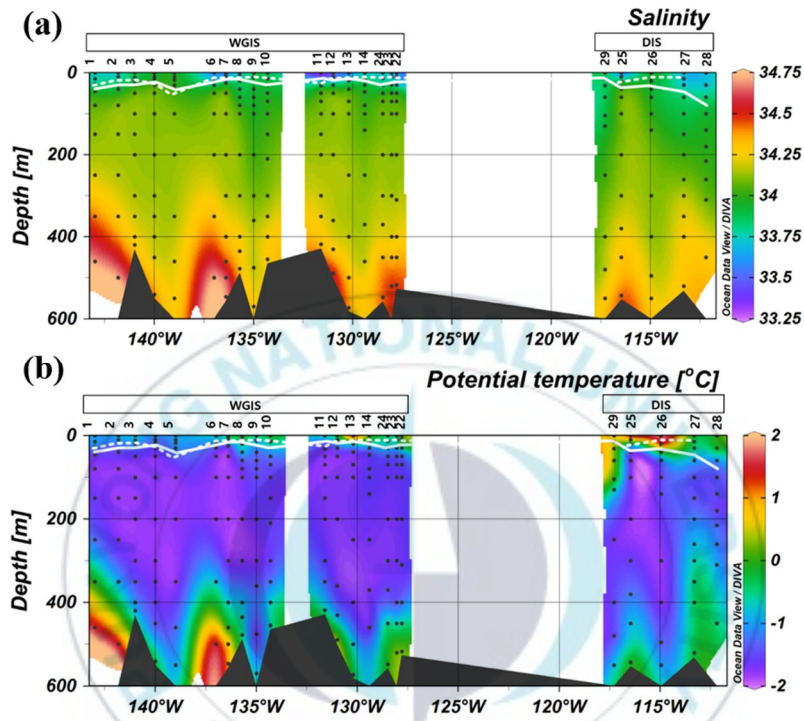


Figure 3. Spatial distributions of (a) salinity and (b) temperature ( $^{\circ}\text{C}$ ) in the WGIS and DIS in the Amundsen Sea. The station numbers are shown at the top of each station. The white dotted lines and white solid lines indicate the euphotic zone depth (EZD) and the mixed layer depth (MLD), respectively.

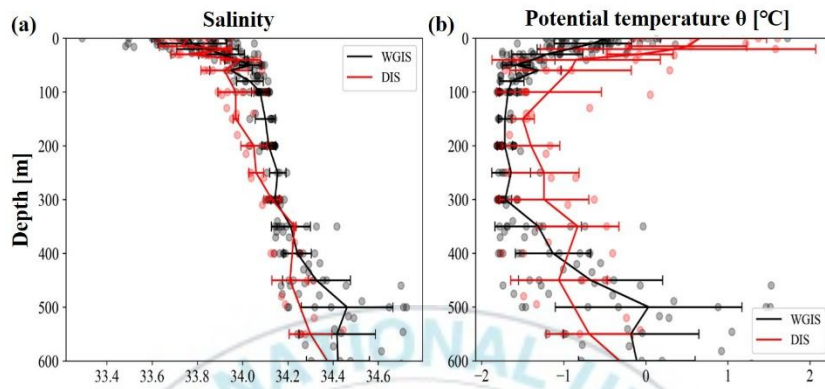


Figure 4. Vertical profiles of salinity and potential temperature ( ) in WGIS and DIS in this study. In WGIS, data were plotted as grey dots, with a black line that represents the mean value, and the error bar representing standard deviations. In DIS, data were plotted as red dots, with a red line that represents the mean value, and the error bar representing standard deviations.

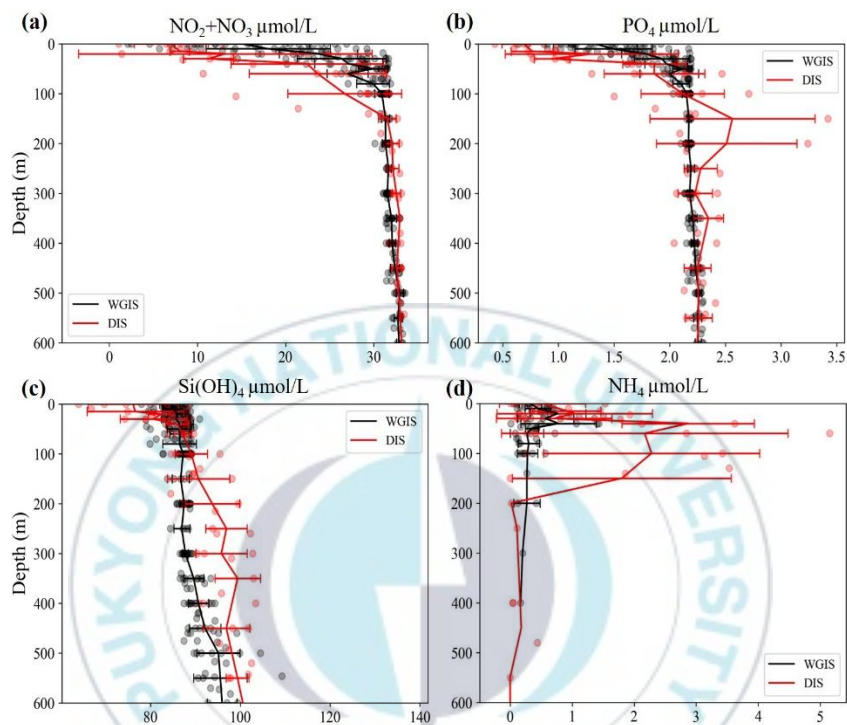


Figure 5. Vertical distributions of (a) nitrate and nitrite ( $\mu\text{mol/L}$ ) ( $\text{NO}_3+\text{NO}_2$ ), (b) phosphate ( $\text{PO}_4$ ), (c) silicic acid ( $\text{Si}(\text{OH})_4$ ), and (d) ammonium ( $\text{NH}_4$ ) in the WGIS and DIS.

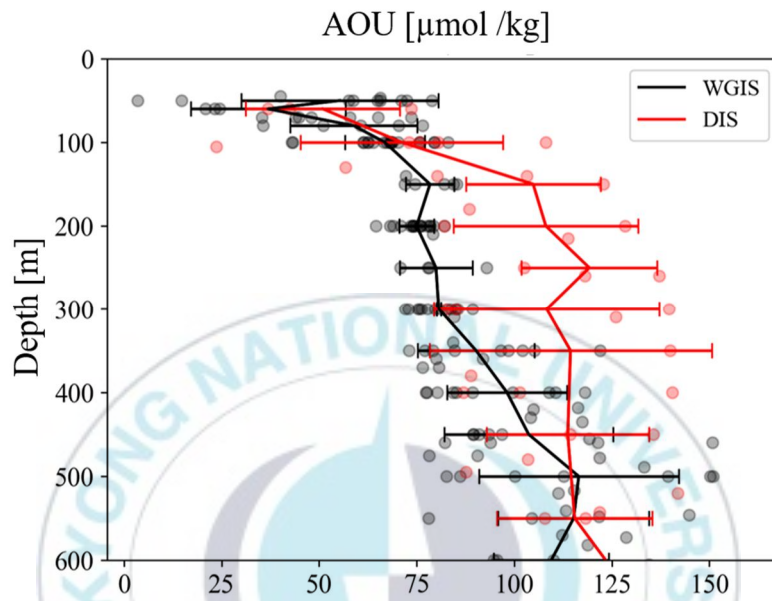


Figure 6. The vertical patterns of AOU ( $\mu\text{mol/kg}$ ) in the WGIS and DIS in the WGIS and DIS, Amundsen Sea.

### 3.2 Distribution of chl *a*

The range of the chl *a* concentration in WGIS was from 0.05 to 15.99 mg/m<sup>3</sup> ( $4.70 \pm 4.45$  mg/m<sup>3</sup>) (Figure 7a). In DIS, the range of the chl *a* concentration was from 0.14 to 19.28 mg/m<sup>3</sup> ( $5.13 \pm 6.00$  mg/m<sup>3</sup>) (Figure 7a). The mean value and range of chl *a* concentration in DIS was higher compared to WGIS. The highest chl *a* concentration was shown in station 27 at 15 m in DIS. In the EZD, the chl *a* concentration was shown in the range from 0.08 to 17.90 mg/m<sup>3</sup>, and the average value was  $7.87 \pm 5.11$  mg/m<sup>3</sup>. Below the EZD, the range of chl *a* concentration was from 0.05 to 19.28 mg/m<sup>3</sup> with an average value of  $3.54 \pm 3.96$  mg/m<sup>3</sup>. The chl *a* concentration was higher in EZD than the below EZD layer. The vertical profile of chl *a* showed the highest concentration in the surface layer and showed a sharp decrease with the depth increased (Figure 7b).



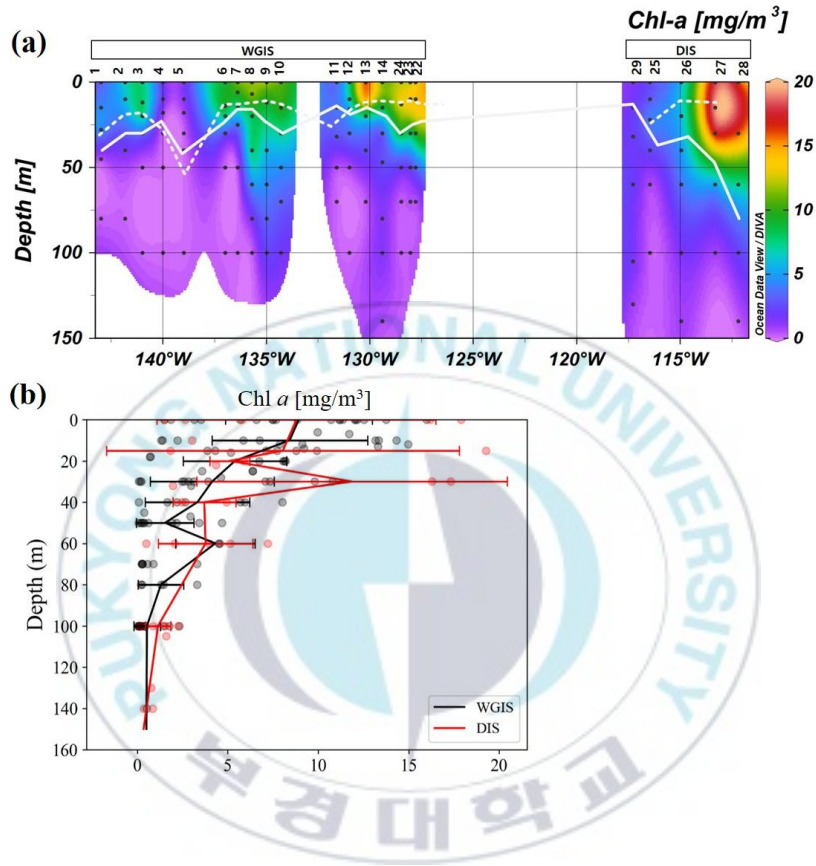


Figure 7. The spatial (a) and vertical profiles (b) of chl *a* ( $\text{mg/m}^3$ ) in the WGIS and DIS. The station numbers are shown at the top of each station.



### 3.3 Distribution of POC

The overall POC concentrations ranged from 3.90 to 77.41  $\mu\text{M C}$  ( $16.87 \pm 16.97 \mu\text{M C}$ ) (Figure 8a). The range of the POC concentrations in WGIS was from 3.90 to 77.41  $\mu\text{M C}$  ( $16.29 \pm 16.56 \mu\text{M C}$ ) (Figure 7a). In DIS, the range of the POC concentrations was from 4.81 to 71.15  $\mu\text{M C}$  ( $18.79 \pm 18.17 \mu\text{M C}$ ) (Figure 7a). There was no difference in the mean value of POC concentrations between WGIS and DIS. The average value of POC in the EZD is  $40.93 \pm 19.27 \mu\text{M C}$  with a range from 6.84 to 77.41  $\mu\text{M C}$ . In the below EZD, the mean value was  $12.22 \pm 12.47 \mu\text{M C}$  with a range from 3.90 to 69.55  $\mu\text{M C}$ . POC concentration showed a high value in the EZD layer and showed a rapid decreasing pattern as the depth increased.

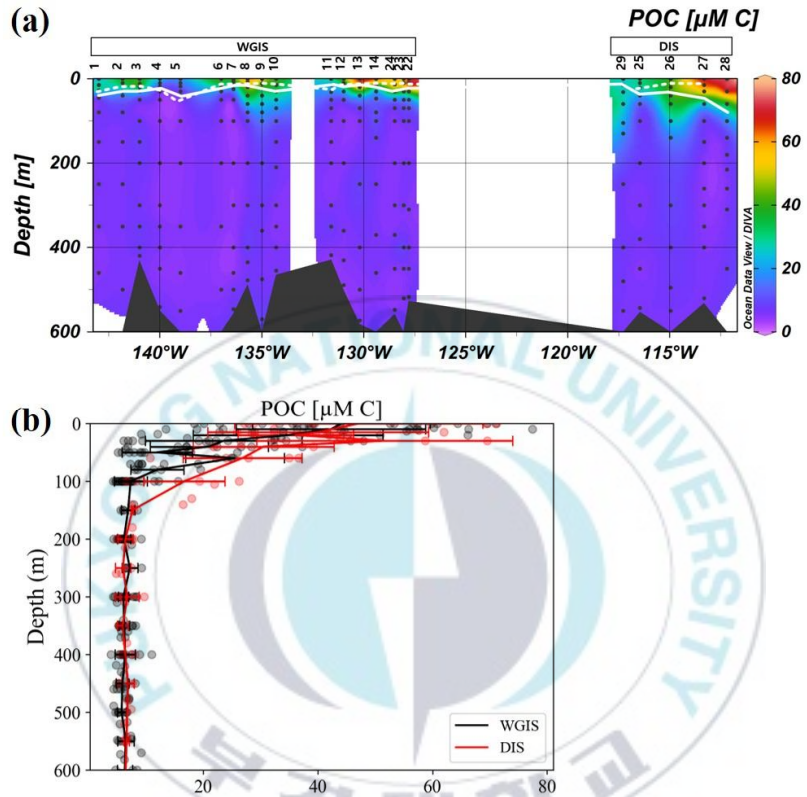


Figure 8. The (a) spatial and (b) vertical profiles of POC ( $\mu\text{M C}$ ) in the WGIS and DIS in the Amundsen Sea.

### 3.4 Distribution of DOC

The range of DOC concentrations was from 36.44 to 70.02  $\mu\text{M C}$  (Figure 9a). The average of DOC concentration was  $43.22 \pm 7.30 \mu\text{M C}$  from all the stations. The range of DOC concentrations in WGIS was from 33.40 to 81.80  $\mu\text{M C}$  (mean:  $43.26 \pm 7.67 \mu\text{M C}$ ) (Figure 9a). In DIS, the range of the DOC concentrations was from 31.09 to 61.96  $\mu\text{M C}$  (mean:  $43.07 \pm 5.97 \mu\text{M C}$ ) (Figure 9a). The range of DOC concentration was wider in WGIS compared to DIS. However, the mean value of DOC concentration did not show any difference. In the EZD, DOC concentrations ranged from 36.44 to 70.02  $\mu\text{M C}$ , and the average value was  $46.87 \pm 7.58 \mu\text{M C}$ . In the below the EZD, the range and average value of DOC concentration were from 31.09 to 81.80 and  $42.27 \pm 7.02 \mu\text{M C}$ , respectively. The DOC profile showed a decreasing pattern as the depth increased (Figure 9b).

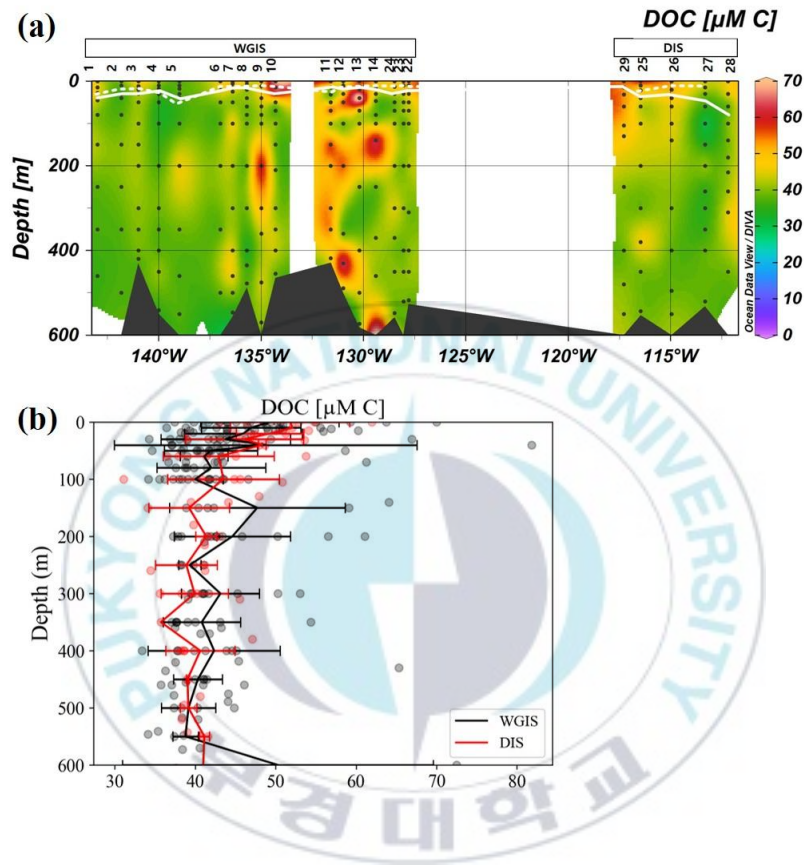


Figure 9. The (a) spatial and (b) vertical profiles of DOC ( $\mu\text{M C}$ ) in the WGIS and DIS in the Amundsen Sea.

### 3.5 Distribution of $a_{350}$

On all profiles, the range of  $a_{350}$  was from 0.01 to 1.44  $\text{m}^{-1}$  (Figure 10a). The average value of  $a_{350}$  was  $0.30 \pm 0.26 \text{ m}^{-1}$ . The highest  $a_{350}$  was shown in 140 m at station 14. The range of  $a_{350}$  concentrations in WGIS was from 0.03 to 1.44  $\text{m}^{-1}$  (mean:  $0.34 \pm 0.27 \text{ m}^{-1}$ ) (Figure 10a). In DIS, the range of the  $a_{350}$  concentrations was from 0.01 to 0.45  $\text{m}^{-1}$  (mean:  $0.14 \pm 0.11 \text{ m}^{-1}$ ) (Figure 10a). The mean value of  $a_{350}$  concentration was higher and the range of  $a_{350}$  concentration was wider in WGIS compared to DIS (Figure 10b). In the EZD,  $a_{350}$  ranged from 0.08 to 1.16  $\text{m}^{-1}$  with an average value of  $0.37 \pm 0.28 \text{ m}^{-1}$ . Below the EZD, the  $a_{350}$  ranged from 0.01 to 1.44  $\text{m}^{-1}$  with an average value of  $0.31 \pm 0.26 \text{ m}^{-1}$ , indicating that there was no significant difference between  $a_{350}$  concentration in EZD and  $a_{350}$  concentration under EZD.

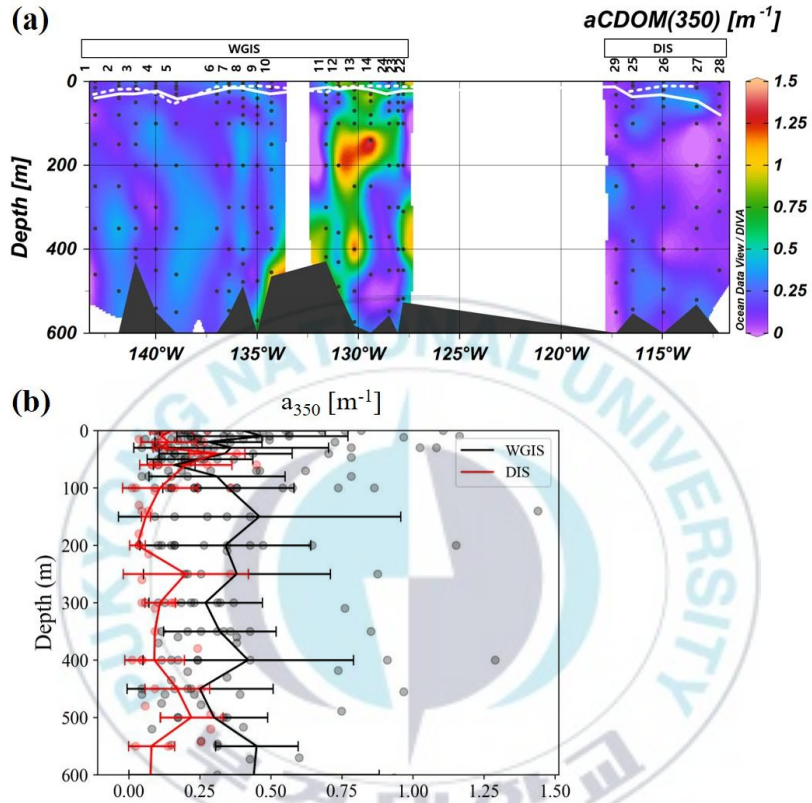


Figure 10. The (a) spatial and (b) vertical profiles of  $a_{350}$  (m<sup>-1</sup>) in the WGIS and DIS in the Amundsen Sea.

### 3.6 Distribution characteristics of FDOM

Two components were identified from the EEMs data of the study area by the PARAFAC model. The optical properties of each component and the comparisons of the results of previous studies are shown in Table 2. The components were identified by the OpenFluor database with Tucker's congruence coefficients, which were higher than 0.95 on the excitation and emission spectra simultaneously.

Based on the excitation-emission maximum, the peaks of a humic-like component (C1) and one protein-like component (C2) were characterized. C1 showed the maximum peak 250 nm for the excitation (Ex) wavelength and 427 nm for the emission (Em) wavelength, which is similar to peak-A introduced by Coble (1996) (Figure 11a). Peak-A represents described as an FDOM<sub>H</sub>, the terrestrial humic-like component, that is derived from the terrestrial substances or organic compounds in soil (Coble, 1996; Stedmon and Bro, 2008; Yamashita and Tanoue, 2008). C2 showed peaks at Ex/Em wavelength of 275/339 (Coble, 1996; Stedmon and Bro, 2008; Yamashita and Tanoue, 2008) (Figure 11b). C2 was similar to the peak-T by Coble (1996) which associated with the autochthonous processes.

The intensity of C1 ranged from 0.010 to 0.031 R.U. with an average value of  $0.017 \pm 0.003$  R.U. (Figure 12a). In WGIS, the intensity of C1



ranged from 0.010 to 0.031 R.U. with an average value of  $0.017 \pm 0.003$  R.U. In DIS, the intensity of C1 ranged from 0.015 to 0.029 R.U. with an average value of  $0.020 \pm 0.003$  R.U. In the EZD, the range of C1 intensity was from 0.010 to 0.023 R.U. with an average value of  $0.015 \pm 0.003$  R.U. Below the EZD, C1 intensity ranged from 0.010 to 0.031 with an average value of  $0.017 \pm 0.003$  R.U. C1 intensity was slightly higher in the below EZD layer compared to the EZD layer (Figure 12a).

On all profiles, the intensity of C2 ranged from 0.001 to 0.049 R.U. with an average value of  $0.007 \pm 0.007$  R.U. (Figure 12b). In WGIS, the intensity of C2 ranged from 0.001 to 0.045 R.U. with an average value of  $0.007 \pm 0.006$  R.U. In DIS, the intensity of C2 ranged from 0.001 to 0.049 R.U. with an average value of  $0.008 \pm 0.009$  R.U. In the EZD, the range of C2 intensity was from 0.003 to 0.049 R.U. with an average value of  $0.011 \pm 0.009$  R.U. Below the EZD, C2 intensity ranged from 0.001 to 0.043 R.U. with the average value of  $0.006 \pm 0.006$  R.U. The highest C2 intensity was shown in the EZD and decreased with depth. The pattern of the vertical distribution of C1 was the reverse of that of C2.



Table. 2

Fluorescent dissolved organic matter (FDOM) of components determined by the PARAFAC model. The components were identified in previous studies from the OpenFluor database

Component	$E_{X_{max}}$ (nm)	$E_{m_{max}}$ (nm)	Coble (1996)	Probable sources	Previous studies
C1	250	427	Peak-A	Terrestrial humic-like associated with soil organic	C2: 225/433 nm (Retelletti Brogi et al., 2018) C1: 250/448 nm (Jeon et al., 2021) C2: 250/430 nm (Painter et al., 2018) C2: <250,320/455 (Retelletti Brogi et al., 2019)
C2	275	339	Peak-T	Protein-like (Tryptophan), Aminoacids; derived from the autochthonous	C3: 270/339.5 (Cabrera et al., 2020) C3: 280/320 (Kim et al., 2020) C3: 275/340 (Stedmon et al., 2011) C3: 275/338 (Retelletti Brogi et al., 2019)

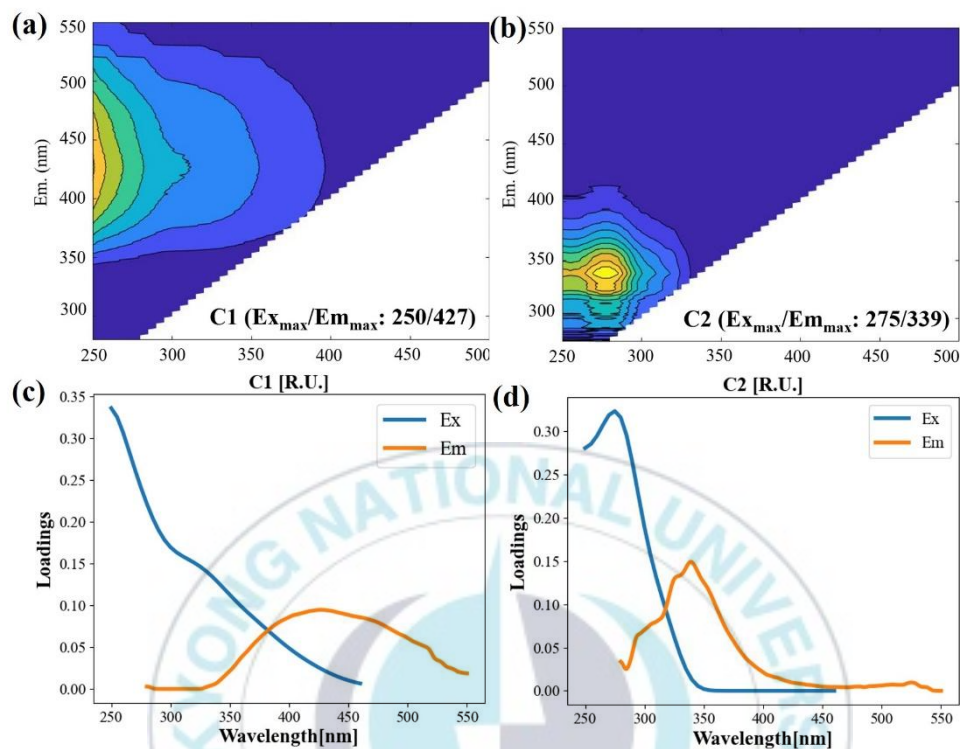


Figure 11. EEM contour plots of the fluorescent spectra of the two components (a) C1 ( $E_{x_{max}}/E_{m_{max}}$ : 250/427, R.U.) and (b) C2 ( $E_{x_{max}}/E_{m_{max}}$ : 275/339, R.U.), identified by PARAFAC analysis in the seawater samples with excitation-emission matrix spectroscopy (EEMs). (c) Loading of C1 and (d) loading of C2 were shown with the blue solid lines representing the excitation wavelength and the orange solid lines representing the emission wavelength.

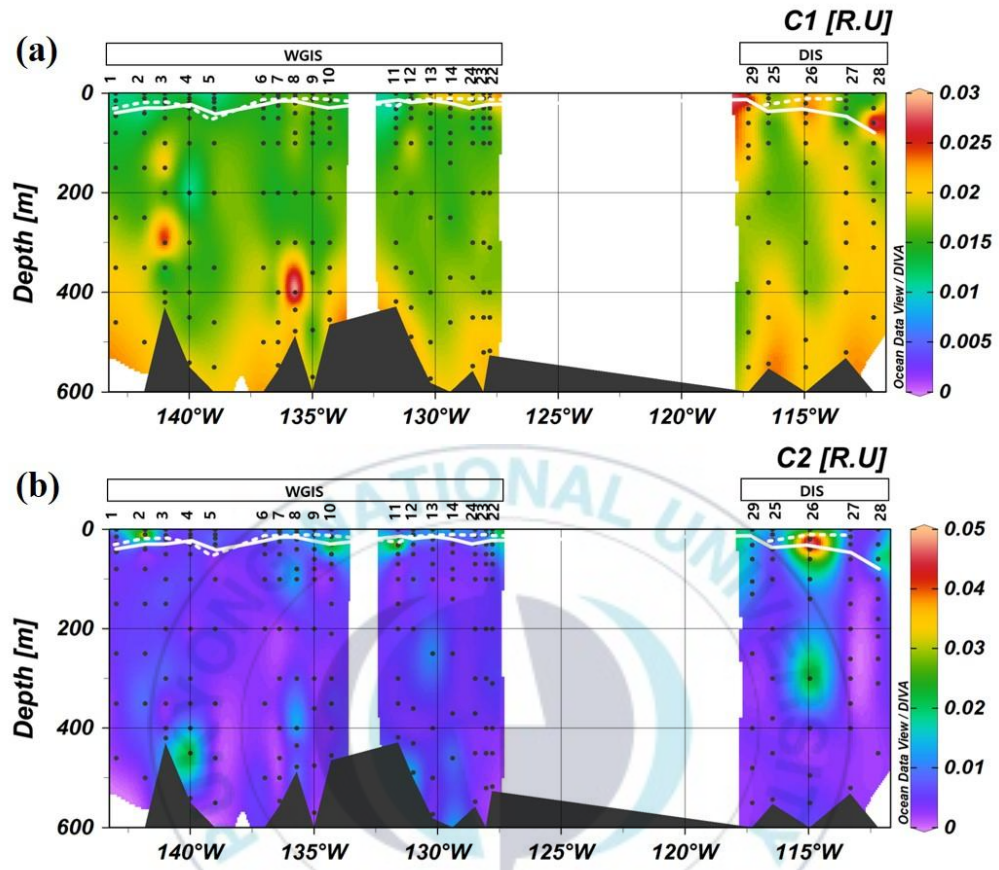


Figure 12. Spatial distributions of (a) C1, and (b) C2 along the west of the Getz ice shelf (WGIS) and the Dotson ice shelf (DIS) in the Amundsen Sea.

### 3.7 Distribution of optical indices of DOM

Optical indices such as  $S_{275-295}$  ( $\text{nm}^{-1}$ ), and  $\text{SUVA}_{254}$  ( $\text{L mg C}^{-1} \text{ m}^{-1}$ ) were evaluated for all samples to characterize the properties of DOM.

$S_{275-295}$  varied from 0.0073 to 0.0506  $\text{nm}^{-1}$  with the average value of  $0.0194 \pm 0.0069$   $\text{nm}^{-1}$  (Figure 13a). In WGIS, the value of  $S_{275-295}$  ranged from 0.0073 to 0.0399  $\text{nm}^{-1}$  with an average value of  $0.0173 \pm 0.0045$   $\text{nm}^{-1}$ . In DIS, the value of  $S_{275-295}$  ranged from 0.0144 to 0.0506  $\text{nm}^{-1}$  with an average value of  $0.0266 \pm 0.0086$   $\text{nm}^{-1}$ . The average value of  $S_{275-295}$  in the DIS was higher than in the WGIS (Figure 13a).

On all profiles, the  $\text{SUVA}_{254}$  varied from 1.22 to 7.39  $\text{L mg C}^{-1} \text{ m}^{-1}$  with an average value of  $2.85 \pm 1.23$   $\text{L mg C}^{-1} \text{ m}^{-1}$  (Figure 13b). In WGIS, the  $\text{SUVA}_{254}$  ranged from 1.22 to 7.39  $\text{L mg C}^{-1} \text{ m}^{-1}$  with a mean value of  $3.08 \pm 1.27$   $\text{L mg C}^{-1} \text{ m}^{-1}$ . In DIS, the  $\text{SUVA}_{254}$  varied from 1.23 to 4.42  $\text{L mg C}^{-1} \text{ m}^{-1}$ , and the average value was  $2.10 \pm 0.67$   $\text{L mg C}^{-1} \text{ m}^{-1}$ . The mean value of  $\text{SUVA}_{254}$  was higher in WGIS compared to DIS (Figure 13b).

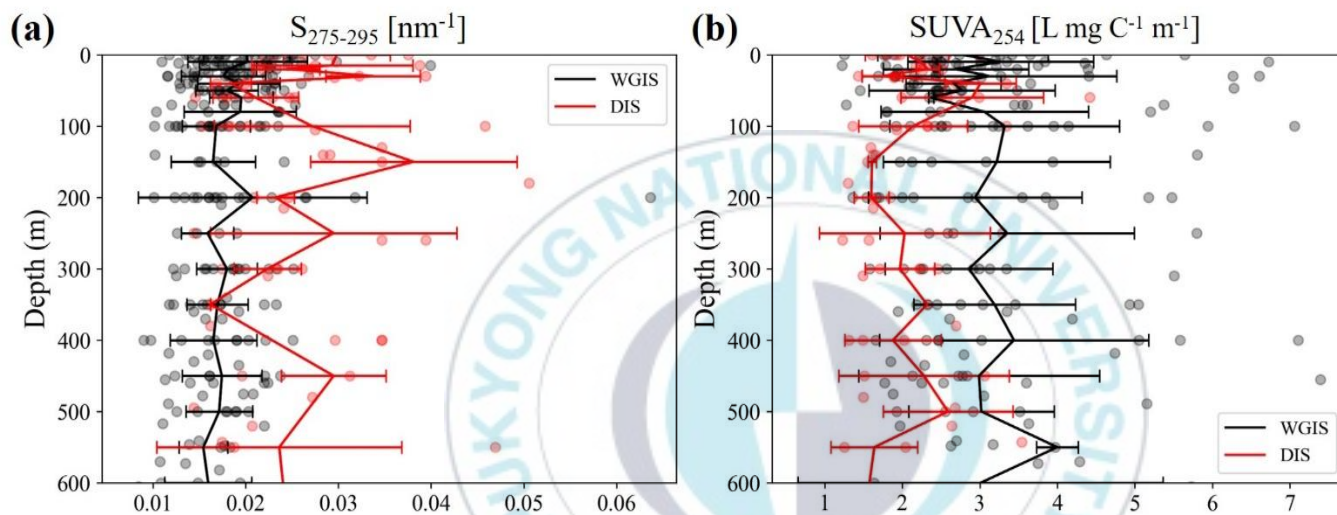


Figure 13. Vertical profiles of  $S_{275-295}$  ( $\text{nm}^{-1}$ ), and  $\text{SUVA}_{254}$  ( $\text{L mg C}^{-1} \text{m}^{-1}$ ) in the WGIS and DIS in the Amundsen Sea.

## . Discussions

### 4.1 Differences in DOM quantity and quality in WGIS and DIS

In order to understand the difference in DOM quantity and quality between WGIS and DIS, the concentration of CDOM and DOC were measured and both  $S_{275-295}$  and  $SUVA_{254}$  were compared in 2020.

In contrast to the DIS (mean:  $0.14 \pm 0.11 \text{ m}^{-1}$ ,  $0.01\text{--}0.45 \text{ m}^{-1}$ ), significantly high concentrations and wide range of  $a_{350}$  were shown in WGIS (mean:  $0.34 \pm 0.27 \text{ m}^{-1}$ ,  $0.03\text{--}1.44 \text{ m}^{-1}$ ) (Figure 10b). Also, a different distribution of DOC concentration was observed. Although mean values of DOC were very similar between WGIS and DIS ( $43.26 \pm 7.67 \text{ }\mu\text{M C}$  in WGIS and  $43.07 \pm 5.97 \text{ }\mu\text{M C}$  in DIS, respectively), the WGIS showed a wider distribution range compared to DIS ( $33.40$  to  $81.80 \text{ }\mu\text{M C}$  in WGIS and  $31.09$  to  $61.96 \text{ }\mu\text{M C}$  in DIS, respectively) (Figure 9b). These results indicate that there is a difference in the concentration and distribution of dissolved organic matter between the WGIS and DIS.

Significant differences in DOM quality between WGIS and DIS were found from  $S_{275-295}$  for average molecular weight (Figure 13a), and  $SUVA_{254}$  for aromaticity (Figure 13b) (Carder et al., 1989; Ohno, 2002; Weishaar et al., 2003). A higher value of  $S_{275-295}$  in DIS ( $0.0266 \pm 0.0086$



$\text{nm}^{-1}$ ) compared to WGIS ( $0.0173 \pm 0.0045 \text{ nm}^{-1}$ ) was observed. This result indicates the predominance of the low molecular weight CDOM in DIS compared in WGIS. WGIS (range:  $1.22\text{--}7.39 \text{ L mg C}^{-1} \text{ m}^{-1}$ , mean:  $3.08 \pm 1.27 \text{ L mg C}^{-1} \text{ m}^{-1}$ ) showed a higher  $\text{SUVA}_{254}$  value of 3 or more and a wider range of  $\text{SUVA}_{254}$  than DIS (range:  $1.23\text{--}4.42 \text{ L mg C}^{-1} \text{ m}^{-1}$ , mean:  $2.10 \pm 0.67 \text{ L mg C}^{-1} \text{ m}^{-1}$ ). This result indicates that the DOM in WGIS is more aromatic than DOM in DIS. This implies that refractory DOM is abundant in WGIS than in DIS.

Figure 14 showed the significant difference in CDOM concentration and CDOM molecular weight between DIS and WGIS in this study. The two regions showed clear difference in CDOM concentration and CDOM molecular weight despite being adjacent study areas. These differences in the DOM quantity and quality between DIS and WGIS might related with the physical differences such as the Antarctic Slope Front (ASF) as reported in the Southern Ocean. The ASF is formed along the Antarctic continental shelf which is associated as a response to Ekman forcing caused by the prevailing easterly wind (Sverdrup, 1953; Muench and Gordon, 1995; Chavanne et al., 2010). The ASF can induce differences in seawater exchange and structure across the Antarctic Front (Large and Yeager, 2009). This difference in ASF structure can affect Antarctic Bottom Water (AABW) formation, primary production, carbon cycle, and

global overturning circulation (Thompson et al., 2018). The ASF can also affect ice shelf basal melting around Antarctica by providing a large source of heat through the transport of the warmer CDW onto the shelf (Fahrbach et al., 1994; Walker et al., 2007; Wåhlin et al., 2010). Previous studies reported that the WGIS was the fresh shelf. Fresh shelf occurred isopycnal gradients of temperature and salinity that has the characteristics of a front separating fresh shelf water from CDW (Dong et al., 2016; Peña-Molino et al., 2016). DIS was the warm shelf that confirmed by a weak easterly wind and eastward Antarctic slope current (ASC), so removing the strong density gradient and shifting the CDW to the continental shelf (Schmidtke et al., 2014; Christie et al., 2018; Thompson et al., 2018; Dotto et al., 2020) (Figure 15). So warm shelf regions can have uninhibited access CDW to the shelf (Jenkins & Jacobs, 2008). Recently, Jeon (2021) reported that humic-like FDOM can be used as a tracer for CDW in the Amundsen Sea. The C1 in this study has a similarity of 0.95 or higher with the C1 study by Jeon (2021) which was confirmed in the OpenFluor online database (Murphy et al., 2014). So, CDW can traced by using C1 which shown in WGIS and DIS (Figure 12a). In WGIS, the distribution of C1 intensity indicated that CDW inflow to the ice shelf, but inflow to the surface was disturbed. C1 intensity in DIS showed that CDW flow into the front of the ice shelf and upwelling to the surface. The two regions, WGIS and DIS,



were affected by the different structures of seawater exchanges. Shen (2018) reported that the degradation of refractory molecules is accelerated by stimulated microbial metabolism and enzyme production when refractory DOC is exposed to a labile substrate. Also, Shen and Benner (2018) reported a decrease in ultraviolet light absorption ( $a_{350}$ ) and an increase in the spectral slope coefficient ( $S_{275-295}$ ) when CDOM is more exposed to solar radiation at the surface through photochemical reaction experiments. In this study, lower  $a_{350}$  and higher  $S_{275-295}$  along with the high  $NH_4$  and AOU that indicated the decomposition and oxygen consumption of organic matter were shown in DIS where CDW flow occurred from the bottom to the surface. So, these results suggest that the difference in the quantity and quality of DOM shown between WGIS and DIS is likely to be the result of the influx of CDW affected by ASF. This difference in the inflow of CDW according to the specific region can influence the biological activity.

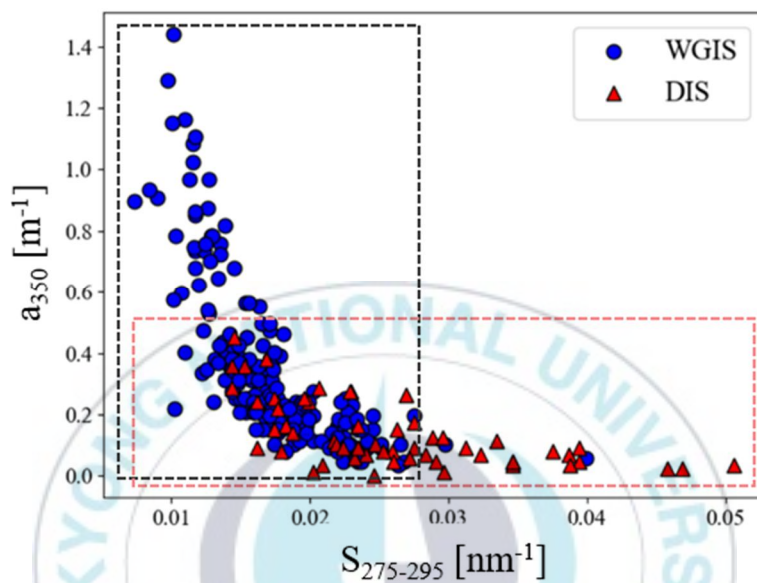


Figure 14. The scatter plot of CDOM absorption coefficient at 350 nm ( $a_{350}$ ,  $\text{m}^{-1}$ ) and CDOM exponential slope values between 275-295 nm ( $S_{275-295}$ ,  $\text{nm}^{-1}$ ). Black dots represent the data of WGIS, and red triangles represent the data of DIS.

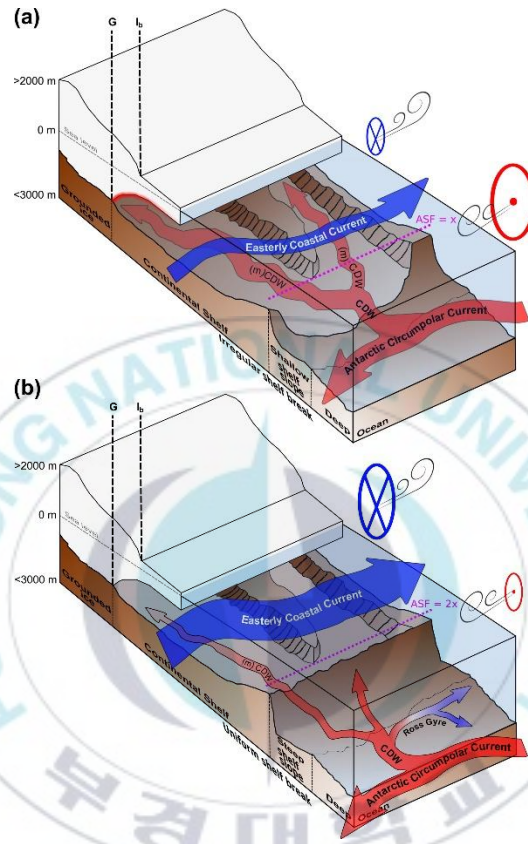


Figure 15. The summary of the oceanic, atmospheric and geologic controls influencing glaciological change along (a) Getz Ice Shelf and (b) the region west of 135 °W (Christie et al., 2018).

## 4.2 Sources of humic-like FDOM in the WGIS and DIS

To identify the source of humic-like FDOM ( $\text{FDOM}_H$ ) in this study area, the relationship between C1 and AOU was plotted (Figure 16). The positive linear relationship between C1 and AOU indicated that the positive linear relationship was primarily attributed to in situ microbial remineralization of sinking organic matter (Yamashita and Tanoue, 2008; Jørgensen et al., 2011; Yamashita et al., 2020). Jørgensen (2011) reported that similar positive linear relationships and slopes were observed in the bathypelagic layer throughout the global ocean except in the North Atlantic. The origin of humic-like FDOM in marine environments can be separated into the autochthonous and allochthonous matter. In order to estimate quantitatively level of autochthonous FDOM, a linear regression model between  $\text{FDOM}_H$  and AOU (Equation 3) was used (Yamashita et al., 2020). The fluorescence intensity of excessive  $\text{FDOM}_H$ , defined as the  $\text{FDOM}_H^*$  was quantified as the difference between the actual measured FDOM and the expected autochthonous FDOM (Equation 4) (Yamashita et al., 2020). Here, I assume that the autochthonous FDOM from  $\text{FDOM}_H$ –AOU relationship follows the process of aerobic remineralization of sinking organic matter. In this study, the expected autochthonous FDOM from  $\text{FDOM}_H$ –AOU relationship in this study was estimated in WGIS and

DIS, since this study area is located in front of the ice shelf among the Antarctic Oceans, and it showed a higher level of  $\text{FDOM}_H$  intensity and AOU values than the previously used relationship (Figure 16). The positive linear relationship in bathypelagic layer in WGIS ( $C1 = 0.9 \times 10^{-4} \text{ AOU} + 9.54 \times 10^{-3}$ ,  $r^2 = 0.45$ ,  $p < 0.05$ ) and DIS ( $C1 = 0.6 \times 10^{-4} \text{ AOU} + 1.3 \times 10^{-2}$ ,  $r^2 = 0.47$ ,  $p < 0.05$ ) was observed. A positive  $\text{FDOM}_H^*$  value indicates the supply of C1 through the sediment (Kim et al., 2018), and the distribution of the pattern from the bottom to the surface was confirmed in WGIS and DIS. These results confirmed that both WGIS and DIS were supplied with  $\text{FDOM}_H$  from sediment. So, these results confirmed that the supply of the humic-like FDOM of both WGIS and DIS is influenced by the supply of humic-like FDOM from sediment at the same time. Since there was no difference in the supply of humic-like FDOM between in front of the WGIS and DIS, the difference in the concentrations and properties of organic matter in front of the west of Getz ice shelf and Dotson ice shelf as independent of the supply of anaerobic  $\text{FDOM}_H$  through sediment.

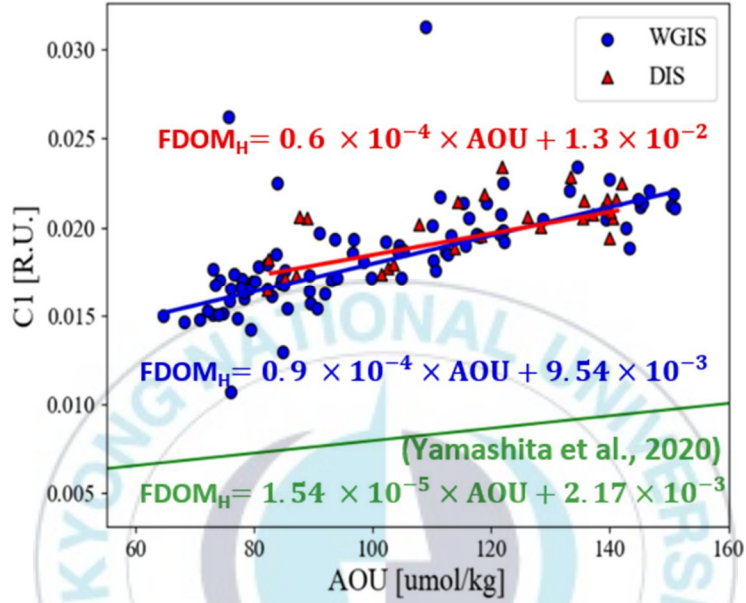


Figure 16. Correlations between C1 (R.U.) and AOU ( $\mu\text{mol/kg}$ ) in the mesopelagic layer (200 m–1000 m) in WGIS ( $\text{C1} = 0.9 \times 10^{-4} \text{AOU} + 9.54 \times 10^{-3}$ ,  $r^2 = 0.45$ ) and DIS ( $\text{C1} = 0.6 \times 10^{-4} \text{AOU} + 1.3 \times 10^{-2}$ ,  $r^2 = 0.47$ ). Black circles represent the samples in WGIS, and red triangles represent the samples in DIS. The reference equation 3 (Yamashita et al., 2020) was represented with a green line.

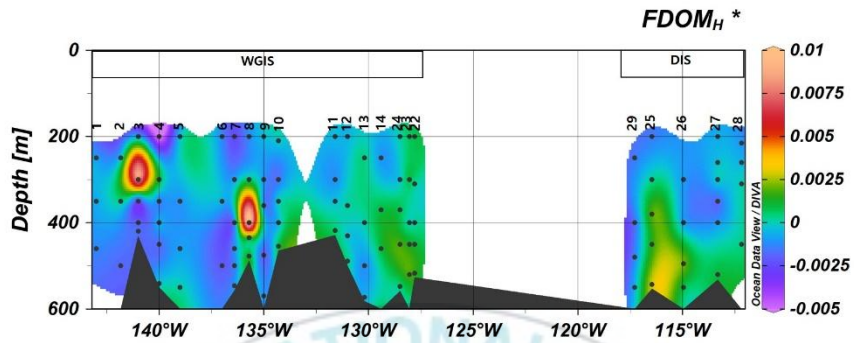


Figure 17. Spatial distributions of  $FDOM_H^*$  along the WGIS and DIS in the Amundsen Sea in Antarctica. Data of autochthonous  $FDOM_H$  and  $FDOM_H^*$  in the upper 200 m is omitted from the figures since it is affected by the air-sea gas exchange of oxygen.



### 4.3 Sources of protein-like FDOM in the WGIS and DIS

In order to investigate the source of protein like FDOM C2 which is known to derive from the autochthonous origin (Stedmon et al., 2011; Retelletti Brogi et al., 2019; Cabrera et al., 2020; Kim et al., 2020), the correlation among C2 %, PO<sub>4</sub> (μM), and POC (uM C) (Figure 18) was examined. The positive correlation between POC and chl *a* ( $y = 3.6228x + 9.9747$ ,  $r^2 = 0.8793$ ) was shown in this study (Figure 19), so POC was used to estimate the phytoplankton carbon biomass. In this study, three groups of distribution in C2 %, PO<sub>4</sub>, and POC relationships were found (Figure 18).

In the first group in this study, C2 % represents about 0 to 20 %, PO<sub>4</sub> represents values between about 2 and 2.5 μM, and POC ranges from about 4.81 to 10 uM C. This group shows high nutrient concentration with low C2 % and low POC concentration at the same time. It means that C2 in first group have been supplied through irrespective of nutrient consumption and biological activity. Through the θ–S diagram (Figure 20) showing the C2 % according to water mass, it was confirmed that 0–20 % of C2 % was mainly present in the WW–CDW mixing line between CDW and WW. This represents the C2 present in CDW and mCDW, and the



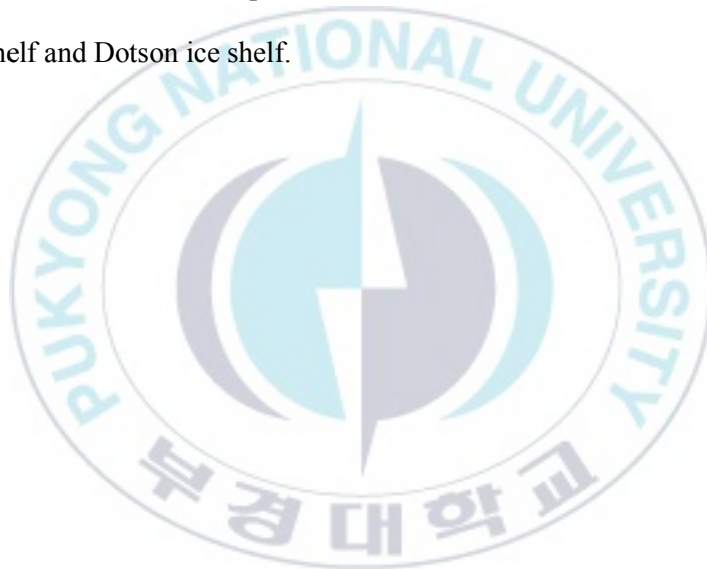
distribution of C2 supplied from the bottom layer due to the inflow of C2 from sediments.

For second group in this study, C2 % represents about 20 to 50 %, PO<sub>4</sub> represents values between about 0.43 and 2.34 uM, and POC ranges from about 4.29 to 77.41 uM C. These results seem to be an increase in C2 % since primary production with a decrease in nutrient concentration and an increase in POC concentration. The second group shows an increase in C2 % with an increase in primary production because nutrients are consumed and the POC concentration increases with primary production. As like the result of this study, CDOM production and a high protein supply of phytoplankton in the Amundsen Sea were reported by Lee et al. (2016) and Song et al. (2016). In second group, the stations in the DIS showed a higher POC than WGIS, which means higher biological production in DIS.

In the third group, C2 % represents about over 50 %, PO<sub>4</sub> represents values between about 0.75 and 2.41 umol/L, and POC ranges from about 4.87 to 59.75 uM C. Although high C2 % was shown, the decrease in nutrient consumption and POC concentration was insignificant. Previous studies reported that the DOM remaining in the ice have a higher protein-like fraction than humic-like DOM fraction (Retelletti-Brogi et al., 2018, Zabłocka et al., 2020). These results indicated C2 % supply by sea ice melt

water and microbial activity or bacterial metabolism independent of nutrient consumption.

A total of three groups representing sources of protein-like FDOM were identified in both WGIS and DIS. So, it was confirmed that there was no difference in the source of protein-like FDOM in front of the west of Getz ice shelf and Dotson ice shelf.



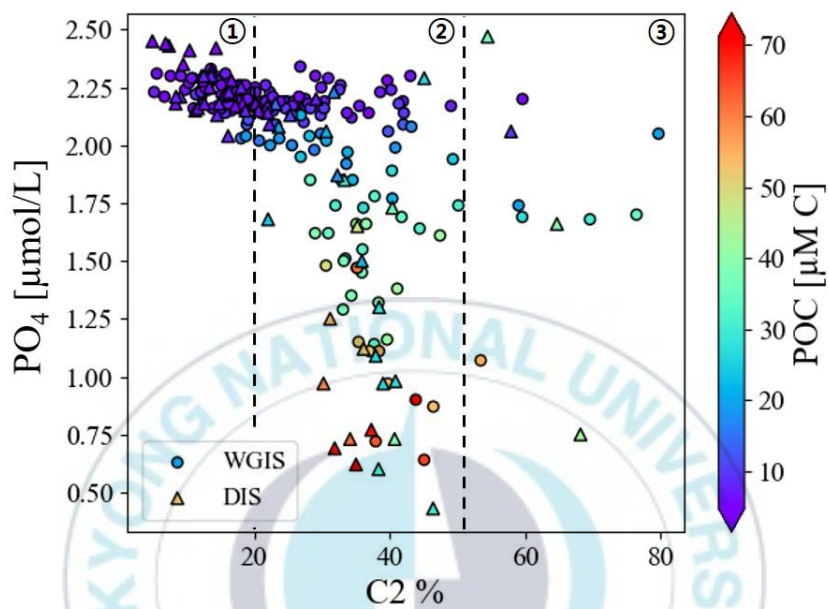


Figure 18. Correlations between C2 % and  $\text{PO}_4$  ( $\mu\text{mol/L}$ ) in the WGIS (circle) and DIS (triangle) in the Amundsen Sea in Antarctica. The color bar shows the POC ( $\mu\text{M C}$ ) concentration.

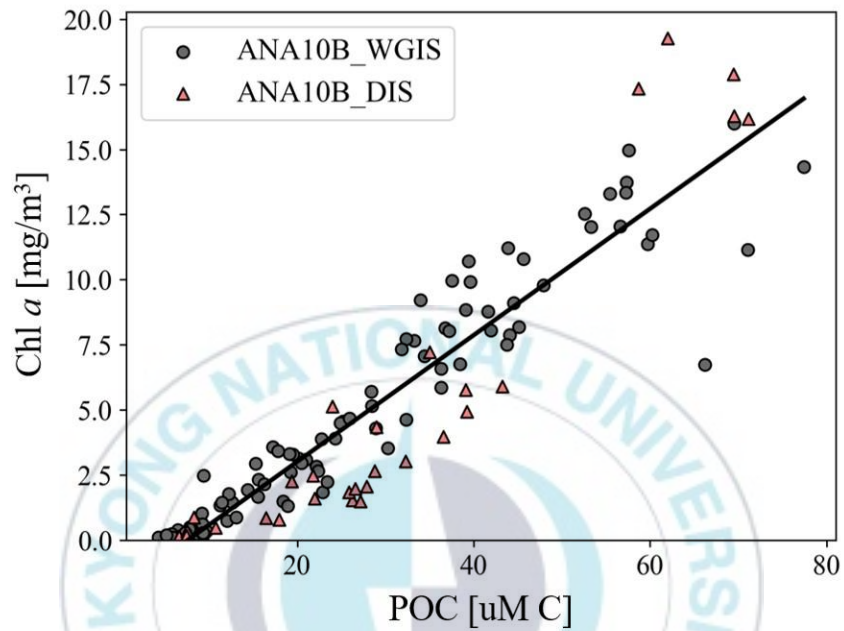


Figure 19. Correlations between POC ( $\mu\text{M C}$ ) and chl *a* ( $\text{mg/m}^3$ ) ( $y = 3.6228x + 9.9747$ ,  $r^2 = 0.8793$ ) in the WGIS and DIS in the Amundsen Sea in Antarctica.

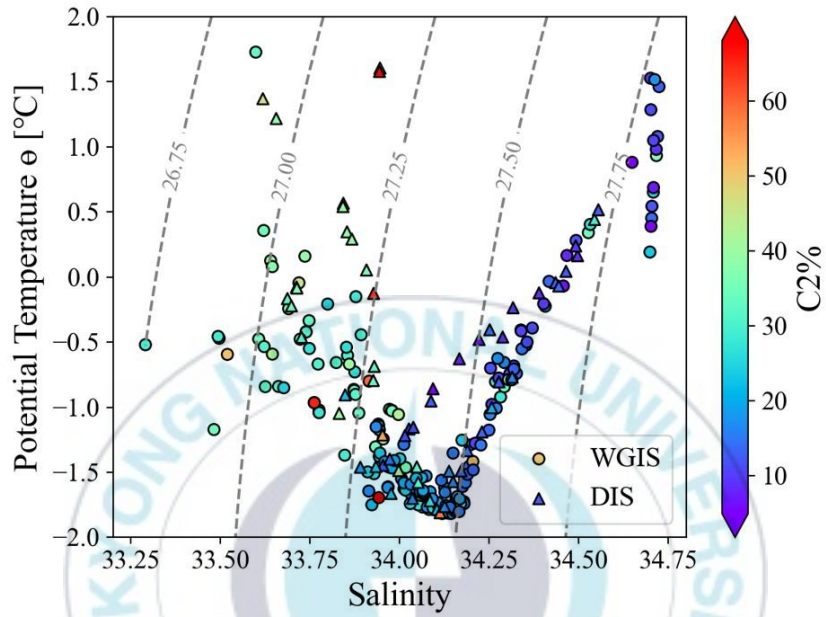


Figure 20. Potential temperature-salinity ( $\theta$ -S) diagram of the sampling stations along the west of the Getz ice shelf (WGIS) (circle) and the Dotson ice shelf (DIS) (triangle) in the Amundsen Sea. The color bar shows the C2 %.

## Conclusion

During a research cruise (ANA10B), from January 6 to February 16 in 2020, at 22 stations, the concentration, characteristics, distribution, and source of DOM were investigated to understand the fluorescence characteristics and dynamics of DOM in front of the West of Getz ice shelf (WGIS) and Dotson ice shelf (DIS) in the Amundsen Sea.

The concentrations of  $a_{350}$  in WGIS and DIS were  $0.34 \pm 0.27 \text{ m}^{-1}$  ( $0.03\text{--}1.44 \text{ m}^{-1}$ ) and  $0.14 \pm 0.11 \text{ m}^{-1}$  ( $0.01\text{--}0.45 \text{ m}^{-1}$ ), respectively, and  $S_{275-295}$  was  $0.017 \pm 0.005 \text{ nm}^{-1}$  ( $0.010\text{--}0.040 \text{ nm}^{-1}$ ) and  $0.027 \pm 0.009 \text{ nm}^{-1}$  ( $0.014\text{--}0.051 \text{ nm}^{-1}$ ) which showing differences in CDOM concentration and molecular weight between WGIS and DIS. The DOC concentrations of WGIS and DIS were  $43.26 \pm 7.67 \text{ }\mu\text{M C}$  ( $33.40\text{--}81.80 \text{ }\mu\text{M C}$ ) and  $43.07 \pm 5.97 \text{ }\mu\text{M C}$  ( $31.09\text{--}61.96 \text{ }\mu\text{M C}$ ), respectively, in WGIS than in DIS. The difference in DOC concentration and optical properties of DOM in front of the western Getz ice shelf and the Dotson ice shelf could be caused by regional differences of CDW which inflows the different routes. The circulation of DOM is influenced by CDW inflows that different from region to region, so this difference resulted a difference in the bioavailability and degradation of DOM. Both in front of the west of Getz ice shelf and Dotson ice shelf were influenced by the supply of humic-like

FDOM through the sediments, and there was no difference between the two regions. So, the differences in DOC concentration and optical properties of DOM do not appear to be related to the supply of anaerobic humic-like FDOM through the sediment. In addition, three groups which contained supply by sediment and other water masses, primary production, and microbial activity were identified as sources of protein-like FDOM in both WGIS and DIS. The source of protein-like FDOM in front of the west of Getz ice shelf and Dotson ice shelf did not show any difference between the two regions. So, the difference in DOC concentration and optical properties of DOM confirmed in front of the western Getz ice shelf and the Dotson ice shelf did not influence by supply of additional source. This difference appears to be difference in the microbial carbon pump according to the inflow of CDW by different routes. The high molecular weight DOM identified in front of the west Getz ice shelf is poorly decomposed and may accumulate and contribute to carbon sequestration. Also, in front of the Dotson ice shelf, DOM can influence the ocean carbon cycle and carbon sequestration as DOM can utilized and removed by biological carbon pumps. This study indicates that CDW intrusion in front of the western Getz ice shelf and the Dotson ice shelf, which are consistently influenced by CDW, also can determine DOM dynamics in the Amundsen Sea and furthermore the carbon cycle in Antarctic. So, it is

necessary to study the distribution and characteristics of DOM through long-term observation because changes in DOM due to climate change can have a significant effect on the carbon cycle in the Antarctic Ocean.





## Reference

- Arrigo, K. R., & Van Dijken, G. L. (2003). Phytoplankton dynamics within 37 Antarctic coastal polynya systems. *Journal of Geophysical Research: Oceans*, 108, 3271–3271.
- Arrigo, K. R., Lowry, K. E., & van Dijken, G. L. (2012). Annual changes in sea ice and phytoplankton in polynyas of the Amundsen Sea, Antarctica. *Deep Sea Research Part II: Topical Studies in Oceanography*, 71, 5-15.
- Asmala, E., Autio, R., Kaartokallio, H., Pitkänen, L., Stedmon, C. A., & Thomas, D. N. (2013). Bioavailability of riverine dissolved organic matter in three Baltic Sea estuaries and the effect of catchment land use. *Biogeosciences*, 10(11), 6969-6986.
- Berggren, M., Laudon, H., & Jansson, M. (2009). Aging of allochthonous organic carbon regulates bacterial production in unproductive boreal lakes. *Limnology and Oceanography*, 54(4), 1333-1342.
- Biddanda, B., & Benner, R. (1997). Carbon, nitrogen, and carbohydrate fluxes during the production of particulate and dissolved organic matter by marine phytoplankton. *Limnology and Oceanography*, 42(3), 506-518.
- Blough, N. V. (1995). Spectroscopic characterization and remote sensing

of non-living organic matter. The role of non-living organic matter in the earth's carbon cycle.

Bricaud, A., Morel, A., & Prieur, L. (1981). Absorption by dissolved organic matter of the sea (yellow substance) in the UV and visible domains. *Limnol. Oceanogr*, 26(1), 43-53.

Brogi, S. R., Ha, S. Y., Kim, K., Derrien, M., Lee, Y. K., & Hur, J. (2018). Optical and molecular characterization of dissolved organic matter (DOM) in the Arctic ice core and the underlying seawater (Cambridge Bay, Canada): Implication for increased autochthonous DOM during ice melting. *Science of the Total Environment*, 627, 802-811.

Bromwich, D. H., Nicolas, J. P., Monaghan, A. J., Lazzara, M. A., Keller, L. M., Weidner, G. A., & Wilson, A. B. (2013). Central West Antarctica among the most rapidly warming regions on Earth. *Nature Geoscience*, 6(2), 139-145.

Cabrera, J. M., Garcia, P. E., Pedrozo, F. L., & Queimaliños, C. P. (2020). Dynamics of the dissolved organic matter in a stream-lake system within an extremely acid to neutral pH range: Agrio-Caviahue watershed. *Spectrochimica Acta Part A: Molecular and Biomolecular Spectroscopy*, 235, 118278.

Carder, K. L., Steward, R. G., Harvey, G. R., & Ortner, P. B. (1989).

- Marine humic and fulvic acids: Their effects on remote sensing of ocean chlorophyll. *Limnology and oceanography*, 34(1), 68-81.
- Catalá, T. S., Reche, I., Fuentes-Lema, A., Romera-Castillo, C., Nieto-Cid, M., Ortega-Retuerta, E., et al & Alvarez-Salgado, X. A. (2015). Turnover time of fluorescent dissolved organic matter in the dark global ocean. *Nature communications*, 6(1), 1-9.
- Cavalieri, D. J., & Parkinson, C. L. (2008). Antarctic sea ice variability and trends, 1979–2006. *Journal of Geophysical Research: Oceans*, 113(C7), C07004
- Chavanne, C. P., Heywood, K. J., Nicholls, K. W., & Fer, I. (2010). Observations of the Antarctic slope undercurrent in the southeastern Weddell Sea. *Geophysical Research Letters*, 37(13), Article L13601
- Chen, M., Jung, J., Lee, Y. K., Kim, T. W., & Hur, J. (2019). Production of tyrosine-like fluorescence and labile chromophoric dissolved organic matter (DOM) and low surface accumulation of low molecular weight-dominated DOM in a productive Antarctic sea. *Marine Chemistry*, 213, 40-48.
- Christie, F. D., Bingham, R. G., Gourmelen, N., Steig, E. J., Bisset, R. R., Pritchard, H. D., et al & Tett, S. F. (2018). Glacier change along West Antarctica's Marie Byrd Land Sector and links to inter-decadal atmosphere–ocean variability. *The Cryosphere*, 12(7), 2461-2479.

- Coble, P. G. (1996). Characterization of marine and terrestrial DOM in seawater using excitation-emission matrix spectroscopy. *Marine chemistry*, 51(4), 325-346.
- Criscitiello, A. S., Das, S. B., Evans, M. J., Frey, K. E., Conway, H., Joughin, I., ... & Steig, E. J. (2013). Ice sheet record of recent sea ice behavior and polynya variability in the Amundsen Sea, West Antarctica. *Journal of Geophysical Research: Oceans*, 118(1), 118-130.
- Dotto, T. S., Naveira Garabato, A. C., Wåhlin, A. K., Bacon, S., Holland, P. R., Kimura, S., ... & Jenkins, A. (2020). Control of the oceanic heat content of the Getz Dotson Trough, Antarctica, by the Amundsen Sea Low. *Journal of Geophysical Research: Oceans*, 125(8), e2020JC016113.
- Eich, C., Biggs, T. E., Poll, W. H., Manen, M. V., Tian, H. A., Jung, J., ... & Brussaard, C. P. (2022). Ecological Importance of Viral Lysis as a Loss Factor of Phytoplankton in the Amundsen Sea. *Microorganisms*, 10(10), 1967.
- Fahrbach, E., Rohardt, G., Schröder, M., & Strass, V. (1994, September). Transport and structure of the Weddell Gyre. In *Annales Geophysicae* (Vol. 12, No. 9, pp. 840-855). Springer-Verlag.
- Fichot, C. G., & Benner, R. (2012). The spectral slope coefficient of

chromophoric dissolved organic matter (S275–295) as a tracer of terrigenous dissolved organic carbon in river influenced ocean margins. *Limnology and Oceanography*, 57(5), 1453-1466.

Frölicher, T. L., Sarmiento, J. L., Paynter, D. J., Dunne, J. P., Krasting, J. P., & Winton, M. (2015). Dominance of the Southern Ocean in anthropogenic carbon and heat uptake in CMIP5 models. *Journal of Climate*, 28(2), 862-886.

Fukuzaki, K., Imai, I., Fukushima, K., Ishii, K. I., Sawayama, S., & Yoshioka, T. (2014). Fluorescent characteristics of dissolved organic matter produced by bloom-forming coastal phytoplankton. *Journal of plankton research*, 36(3), 685-694.

Galletti, Y., Gonnelli, M., Brogi, S. R., Vestri, S., & Santinelli, C. (2019). DOM dynamics in open waters of the Mediterranean Sea: New insights from optical properties. *Deep Sea Research Part I: Oceanographic Research Papers*, 144, 95-114.

Gerringa, L. J., Alderkamp, A. C., Laan, P., Thuroczy, C. E., De Baar, H. J., Mills, M. M., ... & Arrigo, K. R. (2012). Iron from melting glaciers fuels the phytoplankton blooms in Amundsen Sea (Southern Ocean): Iron biogeochemistry. *Deep Sea Research Part II: Topical Studies in Oceanography*, 71, 16-31.

Gordon, L. I., Jennings Jr, J. C., Ross, A. A., & Krest, J. M. (1993). A

suggested protocol for continuous flow automated analysis of seawater nutrients (phosphate, nitrate, nitrite and silicic acid) in the WOCE Hydrographic Program and the Joint Global Ocean Fluxes Study. WOCE hydrographic program office, methods manual WHPO, (68/91), 1-52.

- Granskog, M. A., Macdonald, R. W., Mundy, C. J., & Barber, D. G. (2007). Distribution, characteristics and potential impacts of chromophoric dissolved organic matter (CDOM) in Hudson Strait and Hudson Bay, Canada. *Continental Shelf Research*, 27(15), 2032-2050.
- Hayase, K., & Shinozuka, N. (1995). Vertical distribution of fluorescent organic matter along with AOU and nutrients in the equatorial Central Pacific. *Marine Chemistry*, 48(3-4), 283-290.
- Yamashita, Y., Tsukasaki, A., Nishida, T., & Tanoue, E. (2007). Vertical and horizontal distribution of fluorescent dissolved organic matter in the Southern Ocean. *Marine Chemistry*, 106(3-4), 498-509.
- Helms, J. R., Stubbins, A., Ritchie, J. D., Minor, E. C., Kieber, D. J., & Mopper, K. (2008). Absorption spectral slopes and slope ratios as indicators of molecular weight, source, and photobleaching of chromophoric dissolved organic matter. *Limnology and oceanography*, 53(3), 955-969.
- Huguet, A., Vacher, L., Relexans, S., Saubusse, S., Froidefond, J. M., &

- Parlanti, E. (2009). Properties of fluorescent dissolved organic matter in the Gironde Estuary. *Organic Geochemistry*, 40(6), 706-719.
- Jacobs, S. S. (1991). On the nature and significance of the Antarctic Slope Front. *Marine Chemistry*, 35(1-4), 9-24.
- Jacobs, S. S., Hellmer, H. H., & Jenkins, A. (1996). Antarctic ice sheet melting in the Southeast Pacific. *Geophysical Research Letters*, 23(9), 957-960.
- Jacobs, S. S., & Comiso, J. C. (1997). Climate variability in the Amundsen and Bellingshausen Seas. *Journal of Climate*, 10(4), 697-709.
- Jacobs, S., Jenkins, A., Hellmer, H., Giulivi, C., Nitsche, F., Huber, B., & Guerrero, R. (2012). The Amundsen Sea and the Antarctic ice sheet. *Oceanography*, 25(3), 154-163.
- Jenkins, A., & Jacobs, S. (2008). Circulation and melting beneath George VI ice shelf, Antarctica. *Journal of Geophysical Research: Oceans*, 113(C4).
- Jenkins, A., Dutrieux, P., Jacobs, S. S., McPhail, S. D., Perrett, J. R., Webb, A. T., & White, D. (2010). Observations beneath Pine Island Glacier in West Antarctica and implications for its retreat. *Nature Geoscience*, 3(7), 468-472.
- Jeon, M. H., Jung, J., Park, M. O., Aoki, S., Kim, T. W., & Kim, S. K. (2021). Tracing circumpolar deep water and glacial meltwater using



- humic-like fluorescent dissolved organic matter in the Amundsen Sea, Antarctica. *Marine Chemistry*, 235, 104008.
- Jørgensen, L., Stedmon, C. A., Kragh, T., Markager, S., Middelboe, M., & Søndergaard, M. (2011). Global trends in the fluorescence characteristics and distribution of marine dissolved organic matter. *Marine Chemistry*, 126(1-4), 139-148.
- Joughin, W. (2014). Journal Comment. *Journal of the Southern African Institute of Mining and Metallurgy*, 114(10), iv-iv.
- Jung, J., Hong, S. B., Chen, M., Hur, J., Jiao, L., Lee, Y., ... & Lee, S. (2020). Characteristics of methanesulfonic acid, non-sea-salt sulfate and organic carbon aerosols over the Amundsen Sea, Antarctica. *Atmospheric Chemistry and Physics*, 20(9), 5405-5424.
- Kahru, M., & Mitchell, B. G. (2001). Seasonal and nonseasonal variability of satellite derived chlorophyll and colored dissolved organic matter concentration in the California Current. *Journal of Geophysical Research: Oceans*, 106(C2), 2517-2529.
- Kim, B., Kim, S.-H., Min, J.-O., Lee, Y., Jung, J., Kim, T.-W., et al. (2022). Bacterial metabolic response to change in phytoplankton communities and resultant effects on carbon cycles in the Amundsen Sea Polynya, Antarctica. *Frontiers in Marine Science*, 9, 1–15.
- Kim, J., Cho, H. M., & Kim, G. (2018). Significant production of humic



- fluorescent dissolved organic matter in the continental shelf waters of the northwestern Pacific Ocean. *Scientific reports*, 8(1), 1-8.
- Kim, J., Kim, Y., Kang, H. W., Kim, S. H., Rho, T., & Kang, D. J. (2020). Tracing water mass fractions in the deep western Indian Ocean using fluorescent dissolved organic matter. *Marine Chemistry*, 218 (2020), Article 103720
- Kinsey, J. D., Corradino, G., Ziervogel, K., Schnetzer, A., & Osburn, C. L. (2017). Formation of chromophoric dissolved organic matter by bacterial degradation of phytoplankton-derived aggregates. *Frontiers in Marine Science*, 4, 430.
- Kirk, J. T. (1988). Solar heating of water bodies as influenced by their inherent optical properties. *Journal of Geophysical Research: Atmospheres*, 93(D9), 10897-10908.
- Kirk, J. T. (1994). *Light and photosynthesis in aquatic ecosystems*. Cambridge university press, 509.
- Lakowicz, J. R. (1999). Introduction to fluorescence. In *Principles of fluorescence spectroscopy*, Springer, Boston, MA, 1-23.
- Large, W., & Yeager, S. G. (2009). The global climatology of an interannually varying air–sea flux data set. *Climate dynamics*, 33(2), 341-364.
- Lee, Y. C., Park, M. O., Jung, J., Yang, E. J., & Lee, S. H. (2016).

- Taxonomic variability of phytoplankton and relationship with production of CDOM in the polynya of the Amundsen Sea, Antarctica. *Deep Sea Research Part II: Topical Studies in Oceanography*, 123, 30-41.
- Min, J. O., Kim, S. H., Jung, J., Jung, U. J., Yang, E. J., Lee, S., & Hyun, J. H. (2022). Glacial Ice Melting Stimulates Heterotrophic Prokaryotes Production on the Getz Ice Shelf in the Amundsen Sea, Antarctica. *Geophysical Research Letters*, 49, 19.
- Muench, R. D., & Gordon, A. L. (1995). Circulation and transport of water along the western Weddell Sea margin. *Journal of Geophysical Research: Oceans*, 100(C9), 18503-18515.
- Murphy, K. R., Stedmon, C. A., Wenig, P., & Bro, R. (2014). OpenFluor—an online spectral library of auto-fluorescence by organic compounds in the environment. *Analytical Methods*, 6(3), 658-661.
- Ohno, T. (2002). Fluorescence inner-filtering correction for determining the humification index of dissolved organic matter. *Environmental science & technology*, 36(4), 742-746.
- Orsi, A. H., Whitworth III, T., & Nowlin Jr, W. D. (1995). On the meridional extent and fronts of the Antarctic Circumpolar Current. *Deep Sea Research Part I: Oceanographic Research Papers*, 42(5), 641-673.

- Osburn, C. L., Retamal, L., & Vincent, W. F. (2009). Photoreactivity of chromophoric dissolved organic matter transported by the Mackenzie River to the Beaufort Sea. *Marine Chemistry*, 115(1-2), 10-20.
- Painter, S. C., Lapworth, D. J., Woodward, E. M. S., Kroeger, S., Evans, C. D., Mayor, D. J., & Sanders, R. J. (2018). Terrestrial dissolved organic matter distribution in the North Sea. *Science of the Total Environment*, 630, 630-647.
- Peña Molino, B., McCartney, M. S., & Rintoul, S. R. (2016). Direct observations of the Antarctic Slope Current transport at 113° E. *Journal of Geophysical Research: Oceans*, 121(10), 7390-7407.
- Pritchard, H., Ligtenberg, S. R., Fricker, H. A., Vaughan, D. G., van den Broeke, M. R., & Padman, L. (2012). Antarctic ice-sheet loss driven by basal melting of ice shelves. *Nature*, 484(7395), 502-505.
- Rignot, E., Bamber, J. L., Van Den Broeke, M. R., Davis, C., Li, Y., Van De Berg, W. J., & Van Meijgaard, E. (2008). Recent Antarctic ice mass loss from radar interferometry and regional climate modelling. *Nature geoscience*, 1(2), 106-110.
- Sabine, C. L., Feely, R. A., Gruber, N., Key, R. M., Lee, K., Bullister, J. L., et al & Rios, A. F. (2004). The oceanic sink for anthropogenic CO<sub>2</sub>. *science*, 305(5682), 367-371.
- Schmidtko, S., Heywood, K. J., Thompson, A. F., & Aoki, S. (2014).

- Multidecadal warming of Antarctic waters. *Science*, 346(6214), 1227-1231.
- Shen, Y., & Benner, R. (2018). Mixing it up in the ocean carbon cycle and the removal of refractory dissolved organic carbon. *Scientific reports*, 8(1), 1-9.
- Song, H. J., Kang, J. J., Kim, B. K., Joo, H., Yang, E. J., Park, J., ... & Lee, S. H. (2016). High protein production of phytoplankton in the Amundsen Sea. *Deep Sea Research Part II: Topical Studies in Oceanography*, 123, 50-57.
- Stammerjohn, S., Massom, R., Rind, D., & Martinson, D. (2012). Regions of rapid sea ice change: An inter hemispheric seasonal comparison. *Geophysical Research Letters*, 39(6), L06501.
- Stedmon, C. A., Markager, S., & Bro, R. (2003). Tracing dissolved organic matter in aquatic environments using a new approach to fluorescence spectroscopy. *Marine chemistry*, 82(3-4), 239-254.
- Stedmon, C. A., & Bro, R. (2008). Characterizing dissolved organic matter fluorescence with parallel factor analysis: a tutorial. *Limnology and Oceanography: Methods*, 6(11), 572-579.
- Stedmon, C. A., Amon, R. M. W., Rinehart, A. J., & Walker, S. A. (2011). The supply and characteristics of colored dissolved organic matter (CDOM) in the Arctic Ocean: Pan Arctic trends and differences.

- Marine Chemistry, 124(1-4), 108-118.
- Sverdrup, H. U. (1953). On conditions for the vernal blooming of phytoplankton. *J. Cons. Int. Explor. Mer.* 18(3), 287-295.
- Takahashi, N., Kodaira, S., Tatsumi, Y., Yamashita, M., Sato, T., Kaiho, Y., et al & Kaneda, Y. (2009). Structural variations of arc crusts and rifted margins in the southern Izu Ogasawara arc-back arc system. *Geochemistry, Geophysics, Geosystems*, 10(9), Q09X08.
- Thompson, A. F., Stewart, A. L., Spence, P., & Heywood, K. J. (2018). The Antarctic Slope Current in a changing climate. *Reviews of Geophysics*, 56(4), 741-770.
- Thurnherr, A. M., Jacobs, S. S., Dutrieux, P., & Giulivi, C. F. (2014). Export and circulation of ice cavity water in Pine Island Bay, West Antarctica. *Journal of Geophysical Research: Oceans*, 119(3), 1754-1764.
- Turner, J., Comiso, J. C., Marshall, G. J., Lachlan Cope, T. A., Bracegirdle, T., Maksym, T., ... & Orr, A. (2009). Non annular atmospheric circulation change induced by stratospheric ozone depletion and its role in the recent increase of Antarctic sea ice extent. *Geophysical Research Letters*, 2009, 36.8.
- Venables, H., & Moore, C. M. (2010). Phytoplankton and light limitation in the Southern Ocean: Learning from high nutrient, high

- chlorophyll areas. *Journal of Geophysical Research: Oceans*, 115(C2), C02015.
- Wåhlin, A. K., Yuan, X., Björk, G., & Nohr, C. (2010). Inflow of warm Circumpolar Deep Water in the central Amundsen shelf. *Journal of physical oceanography*, 40(6), 1427-1434.
- Walker, D. P., Brandon, M. A., Jenkins, A., Allen, J. T., Dowdeswell, J. A., & Evans, J. (2007). Oceanic heat transport onto the Amundsen Sea shelf through a submarine glacial trough. *Geophysical Research Letters*, 34(2), L02602.
- Weishaar, J. L., Aiken, G. R., Bergamaschi, B. A., Fram, M. S., Fujii, R., & Mopper, K. (2003). Evaluation of specific ultraviolet absorbance as an indicator of the chemical composition and reactivity of dissolved organic carbon. *Environmental science & technology*, 37(20), 4702-4708.
- Westerhoff, P., Chao, P., & Mash, H. (2004). Reactivity of natural organic matter with aqueous chlorine and bromine. *Water Research*, 38(6), 1502-1513.
- Yager, P. L., Sherrell, R. M., Stammerjohn, S. E., Alderkamp, A. C., Schofield, O., Abrahamsen, E. P., et al & Wilson, S. (2012). ASPIRE: the Amundsen Sea Polynya international research expedition. *Oceanography*, 25(3), 40-53.

- Yamashita, Y., & Tanoue, E. (2008). Production of bio-refractory fluorescent dissolved organic matter in the ocean interior. *Nature Geoscience*, 1(9), 579-582.
- Yamashita, Y., Jaffé, R., Maie, N., & Tanoue, E. (2008). Assessing the dynamics of dissolved organic matter (DOM) in coastal environments by excitation emission matrix fluorescence and parallel factor analysis (EEM PARAFAC). *Limnology and oceanography*, 53(5), 1900-1908.
- Yamashita, Y., Nishioka, J., Obata, H., & Ogawa, H. (2020). Shelf humic substances as carriers for basin-scale iron transport in the North Pacific. *Scientific reports*, 10(1), 1-10.
- Yamashita, Y., Tosaka, T., Bamba, R., Kamezaki, R., Goto, S., Nishioka, J., ... & Ogawa, H. (2021). Widespread distribution of allochthonous fluorescent dissolved organic matter in the intermediate water of the North Pacific. *Progress in Oceanography*, 191, 102510.
- Zepp, R. G., Sheldon, W. M., & Moran, M. A. (2004). Dissolved organic fluorophores in southeastern US coastal waters: correction method for eliminating Rayleigh and Raman scattering peaks in excitation–emission matrices. *Marine chemistry*, 89(1-4), 15-36.